iScience

CellPress
OPEN ACCESS

Article

# Dynamic intracellular mechanical cues facilitate collective signaling responses

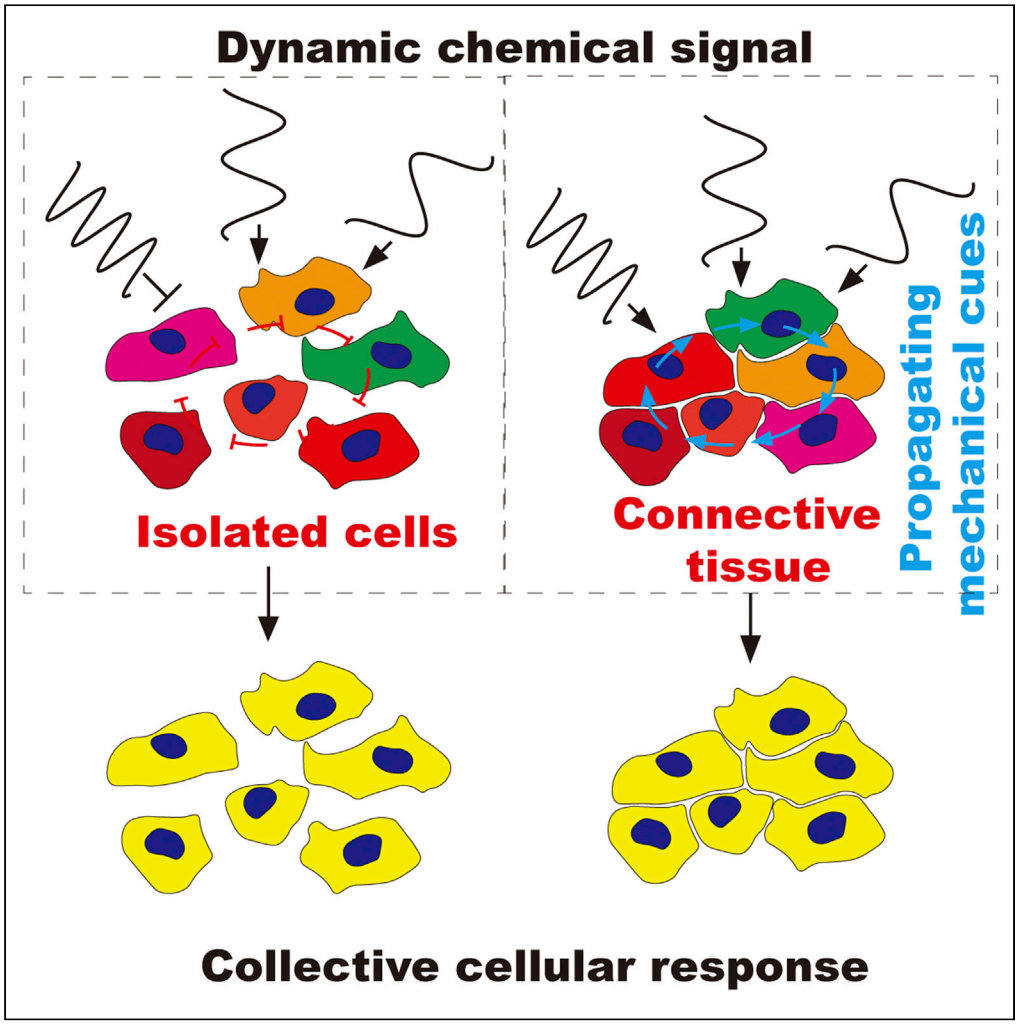


Bingchen Che, Wei Zhao, Yanan Liu, ..., Jintao Bai, Xiqiao Feng, Ce Zhang

jing@nwu.edu.cn (G.J.)
zhangce.univ@gmail.com (C.Z.)

## Highlights

Dynamic intracellular mechanical cues facilitate collective cellular responses

The dynamic chemical stimulations are translated into intracellular mechanical cues

The synergy between dynamic mechanical and chemical signal plays crucial roles

Che et al., iScience *24*, 102396
May 21, 2021 
https://doi.org/10.1016/j.isci.2021.102396

iScience

CellPress
OPEN ACCESS

Article

# Dynamic intracellular mechanical cues facilitate collective signaling responses

Bingchen Che,[1] Wei Zhao,[1] Yanan Liu,[2] Dan Sun,[1] Guangyin Jing,[2,*] Jintao Bai,[1] Xiqiao Feng,[3] and Ce Zhang[1,4,*]

## SUMMARY

**Collective behavior emerges in diverse life machineries, e.g., the immune responses to dynamic stimulations. The essential questions that arise here are that whether and how cells *in vivo* collectively respond to stimulation frequencies higher than their intrinsic natural values, e.g., the acute inflammation conditions. In this work, we systematically studied morphological and signaling responses of population fibroblasts in an interconnected cell monolayer and uncovered that, besides the natural NF-$\kappa$B oscillation frequency of 1/90 min$^{-1}$, collective signaling response emerges in the cell monolayer at 1/20 min$^{-1}$ TNF-$\alpha$ input periodicity as well. Using a customized microfluidic device, we independently induced dynamic chemical stimulation and cytoskeleton reorganization on the stand-alone cells to exclude the effect of cell-cell communication. Our results reveal that, at this particular frequency, chemical stimulation is translated into dynamic intracellular mechanical cues through RAC1-medicated induction of dynamic cell-cell connections and cytoskeleton reorganizations, which synergize with chemical input to facilitate collective signaling responses.**

## INTRODUCTION

Collective behavior is the outcome of interactions among individual cells. The short-range cell-cell and cell-extracellular matrix (ECM) interactions allow the living tissues to undergo drastic behavioral transitions for biological functions such as migration, embryogenesis, and tumorigenesis (Roure et al., 2005; Lecaudey and Gilmour, 2006; Friedl and Wolf, 2003). The intra-cellular signaling activities are typically heterogeneous among population cells. The otherwise random signaling cascade of population cells gets coordinated by tuning the fluctuating external signals to its natural frequency (Tay et al., 2010) or through cell-cell communication to synchronize their responses (Sun et al., 2012). For example, Sun et al. reveal that collective calcium responses emerge in the crowded cell population when cells communicate via gap junctions upon ATP stimulation, leading to faster, more synchronized, and highly correlated responses as compared with the stand-alone (SA) cells.

In the crowded cellular environment of biological tissues, the local tissue architecture (Box et al., 2019) and the motion and deformation dynamics of individual cells (Pan et al., 2016) generate propagating physical signals, which affect intracellular signaling cascades. Numerous studies reveal that the physical characters of cellular micro-environment affect the long-term cellular activities associated with cell fate, including cell polarization (Copos and Mogilner, 2020; Asnacios and Hamant, 2012), division (Floris et al., 2012; Gudipaty et al., 2017), and differentiation (He et al., 2018). But the regulatory effects of mechanical cues on short-term cellular behavior, e.g., immune responses, remain unresolved. Schrader et al. reveal that abnormal ECM stiffness causes intracellular structural changes at the cytoskeleton-membrane interface and thereby blocks the transient signaling responses to targeting drugs (Frangogiannis, 2016). The fibroblast-collagen matrix can set free soluble cytokines under external mechanical actuations, which activate intra-cellular signaling pathways (Wells and Discher, 2008). These results indicate that dynamic mechanical cues resulting from inter-cell interactions can affect the intra-cellular activities. How mechanical cues facilitate population cells adapting to the ever-changing chemical environment and the correlation between collective cellular behaviors and optimal tissue functions remain unexplored.

In this work, we studied the effects of dynamic intracellular mechanical cues, which result from the collective morphological responses, on the signaling activities of population cells in an interconnected cell monolayer (ICM). By tuning the TNF-$\alpha$ input periodicities, we observed that fibroblasts in ICM show substantially

[1]State Key Laboratory of Photon-Technology in Western China Energy, Institute of Photonics and Photon-Technology, Northwest University, Xi'an 710069, China

[2]School of Physics, Northwest University, Xi'an 710069, China

[3]Institute of Biomechanics and Medical Engineering, Department of Engineering Mechanics, Tsinghua University, Beijing 100084, China

[4]Lead contact

*Correspondence: jing@nwu.edu.cn (G.J.), zhangce.univ@gmail.com (C.Z.)

https://doi.org/10.1016/j.isci.2021.102396

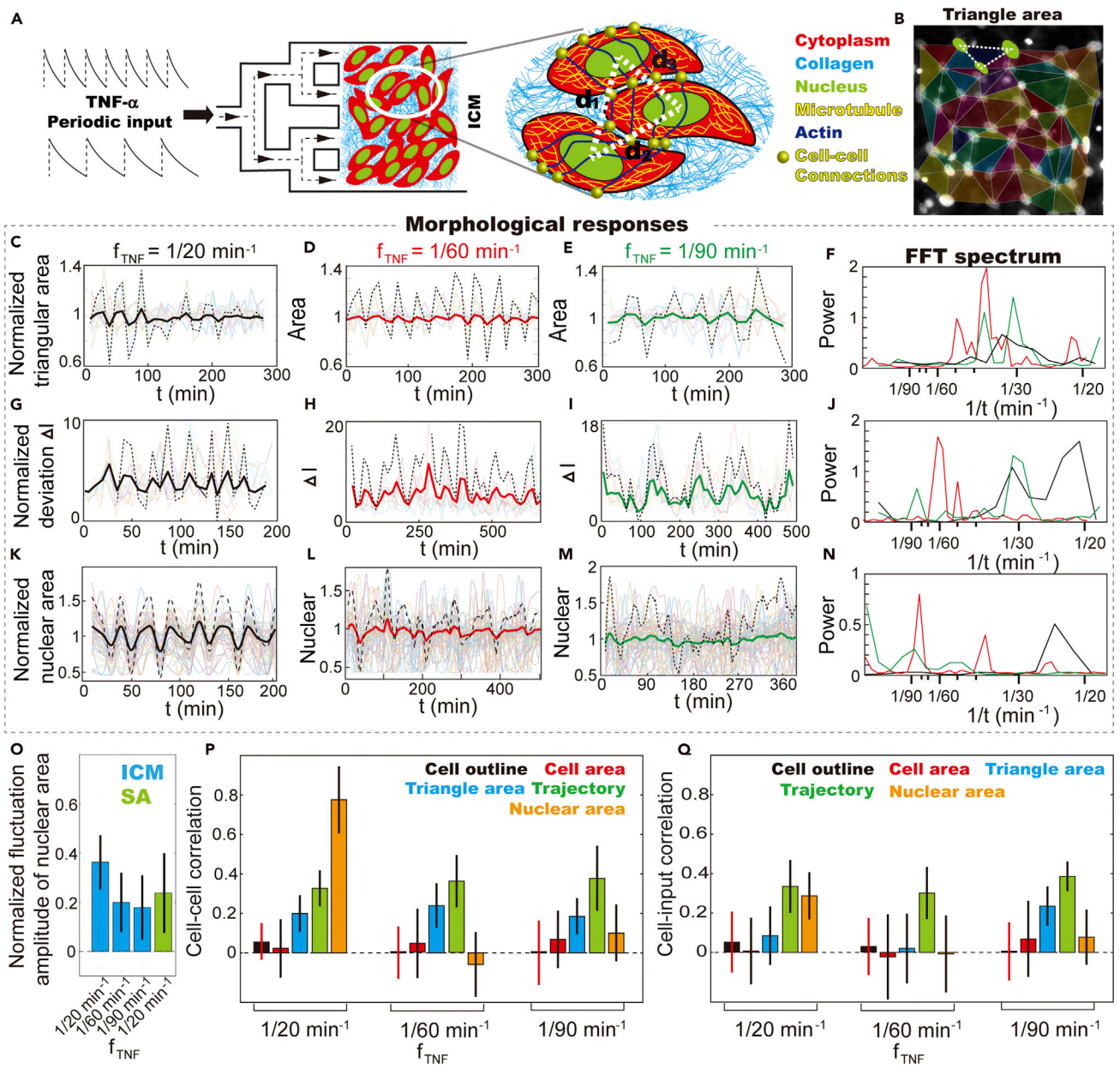


**Figure 1. Collective morphological response of population cells in ICM upon periodic TNF-α stimulation**

(A) Schematic showing that the ICM was maintained in a microfluidic culture chamber and stimulated by dynamic TNF-α inflammatory signal of various amplitudes and frequencies.

(B) Cell-cell interactions are evaluated by measuring the triangular area connecting three neighboring cells.

(C–E) Relative displacement of the nucleus with respect to the neighbors causes changes in the triangular area, which reflect the cell-cell and cell-ECM interactions. The traces were normalized by their average value. The translucent lines are traces of individual cells. The solid line is the average of all traces, and the dashed line is the enlarged view of the solid line for better visualization of the fluctuation.

(F) Fast Fourier transform (FFT) shows that variations in the triangular area at all TNF-α input periodicities share a similar dominant frequency, ranging from 1/40 to 1/30 $min^{-1}$

(G–I) Collective vibration of nuclear centroid during cell migration within the ICM reflects deformation of the cell monolayer, which coordinates with periodic TNF-α stimulation. The traces were normalized by their average value. The translucent lines are traces of individual cells. The solid line is the average of all traces, and the dashed line is the enlarged view of the solid line for better visualization of the fluctuation.

(J) Fast Fourier transform (FFT) shows that the dynamic ICM deformation synchronizes with TNF-α input.

(K–M) Nuclear shape fluctuation (NSF) traces of single fibroblasts in the ICM upon stimulation. The traces were normalized by their average value. The translucent lines are traces of individual cells. The solid line is the average of all traces, and the dashed line is the enlarged view of the solid line for better visualization of the fluctuation.

**Figure 1. *Continued***

(N) Fast Fourier transform (FFT) shows dominant NSF frequency between 1/20 and 1/30 $min^{-1}$, when stimulated by 1/20 $min^{-1}$ TNF-α stimulation.

(O) Fluctuation amplitude of nuclear shape changes in ICM and the stand-alone (SA) cells upon periodic TNF-α stimulation. The fluctuation amplitude of individual cells' nucleus was normalized to its time averaged area. The error bars represent standard deviation of population cell's fluctuation amplitude in nuclear area.

(P) Cross-correlation analysis of the morphological responses of population cells in the ICM reveals that the collective behavior is most obvious in NSF when stimulated by 1/20 $min^{-1}$ TNF-α input. The error bars represent standard deviation of the correlation coefficients between any 2 neighboring cells in a population.

(Q) Cross-correlation analysis between the morphological responses of population cells in the ICM and TNF-α periodic stimulations reveal that contractile activities of ICM as a whole entity coordinate with TNF-α stimulation. The error bars represent standard deviation of the correlation coefficients between individual cells and the TNF-α input.

different morphological and signaling responses as compared with the SA cells. Collective signaling activities emerge in ICM at both 1/20 and 1/90 $min^{-1}$ TNF-α inputs and only at the natural frequency of NF-κB signaling cascade for SA cells (i.e., 1/90 $min^{-1}$). Meanwhile, at the particular frequency of 1/20 $min^{-1}$, the dynamic loss and re-establishment of cell-cell connections mediated by elevated RAC1 expression generates intracellular mechanical cues, which causes collective nuclear shape changes in ICM. Using a customized microfluidic device, we reconstructed the cytoskeleton reorganization and simultaneously introduced dynamic TNF-α stimulations to the SA cells, which sophisticatedly excludes the effect of chemical information exchange. It is surprising that we found the collective behaviors within the biological tissues is a consequence of the synergy between cell-cell interactions, mechano-signaling, and NF-κB dynamics. Phase mismatching among those factors leads to disrupted collective behavior. We, therefore, conclude that the on-off process of cell-cell connections provides a feedback loop, where dynamic intracellular mechanical cues caused by TNF-α-induced cytoskeleton reorganization facilitate collective cellular responses to dynamic chemical stimulations. This investigation reveals a novel cascade process linking the morphological and signaling collective behaviors and provides opportunities to develop novel therapeutic strategies, utilizing controllable mechanical cues to manipulate tissue function *in vivo*.

## RESULTS AND DISCUSSION

### Morphological responses of population cells in ICM under periodic TNF-α stimulation

To model the crowded cellular environment in the biological tissue, we cultured high-density 3T3 fibroblasts in a shear-free microfluidic culture chamber (Figures 1A and S1). Using the integrated peristaltic pumps, nutrients and drugs loaded from the inlets can be driven to designated channels and culture chambers within tens of seconds (Zhang et al., 2019). With prolonged incubation, the fibroblasts self-organize into a compact monolayer sheet, i.e., the ICM, in which the mobility of most cells decreases dramatically (Figures S2A and S2B, Videos S1 and S2). The space between cells is filled by collagen secreted by fibroblasts (Figure S2E). The mechanical cues caused by nuclear translocation and shape transition can, therefore, be effectively transduced to the neighbors through remodeling of microtubule networks (Figures S2A–S2L and supplementary information). In the meantime, the collective movement of population cells in the ICM is regulated through the interconnective actin filaments, resulting in a correlation length of ~70 μm (Figures S2M–S2S). These results indicate that, when cell density exceeds 700 cell/$mm^2$, the landscape of mechanical cues from one cell are transmitted over distances spanning multiple cell size (supplementary information). The dynamic inter- and intra-cellular mechanical cues in ICM can thus be quantified by monitoring the morphological responses of individual cells.

After the ICM was stabilized in the culture chamber, dynamic inflammatory signals of various frequencies and amplitudes were introduced to mimic the everchanging cellular environment *in vivo* (Figures 1A and S1D–S1F). In the meantime, we monitored the morphological responses of individual cells in ICM, i.e., the cell outline and surface area reflecting line strain and surface tension; the nuclear shape reflecting changes in the compressive forces caused by cytoskeleton reorganization; and the triangular area connecting three nuclear reflecting cell-cell interactions (Figures 1A, 1B, and S2T–S2V, supplementary information). Our results demonstrate that hints of collective activities emerge only in some of the morphological features. The coordinated variations of the triangle area at all TNF-α input frequencies leads to a correlation coefficient of ~0.2 (Figures 1B–1E) (Figure 1P). The dynamic variations suggest the emergence of synchronized mechanical cues from neighboring cells, the intracellular cytoskeleton reorganization (Harris, 2012; Khalilgharibi et al., 2019), and, to some extent, the collective movement of the interconnective actin layer (Video S3). It is intriguing that the variations in the triangle area do not coordinate with the periodic TNF-α stimulation (Figure 1Q). Instead, Fast Fourier transform spectrums show dominant frequencies between

1/30 and 1/40 $min^{-1}$ regardless of TNF-$\alpha$ input periodicities (Figure 1F), suggesting that the frequency is an intrinsic character of ICM. In contrast, the morphological responses of individual cells (i.e., the cell outline and 2D projected area) are highly heterogeneous and random with dynamic TNF-$\alpha$ stimulations (Figures 1P, 1Q, S3A–S3F, and S4), reflecting mechanical cues received at the cell-cell and cell-ECM interfaces, which are timely and spatially uncoordinated among population cells. Consistently, in the time series of neighboring cells, the cross-correlation analysis reveals that the correlation coefficients of cell outline and surface area are close to zero, which are considerably smaller than that of the triangular area (Figure 1P and supplementary information).

The collective movement of population cells in ICM is disrupted by the addition of TNF-$\alpha$. ICM of different sizes exhibit distinctive morphological responses (Figures S3G and S4). A small ICM (i.e., small quantities of cells) exhibits contractile behavior upon periodic TNF-$\alpha$ stimulation, resulting in a decrease in the overall size (Video S4). Of note, the contractile behavior starts at the marginal area (Figures S3H–S3K and Video S5). Subsequently, the dissembling of cell-ECM and cell-cell connections leads to decreased mechanical loads on the nucleus (Kim et al., 2015; Zhang et al., 2020). When the ICM is overly crowded in a confined space (i.e., >80 cells in the culture chamber of 400 $\mu$m × 400 $\mu$m in size), the size of the ICM remains unchanged during periodic TNF-$\alpha$ stimulation. Instead, collective oscillatory movement of nuclear and actin filaments emerges, which suggests dynamic variations in the local stress of actin networks (Figures S3I–S3K and S4). To evaluate the TNF-$\alpha$-stimulated contractile actions of ICM, we measured the deviation of migration coordinates of individual cells from the averaged trajectory, $\Delta I$ (supplementary information). We observed that population cells share a similar vibrating frequency despite their distinctive long-distance migration trajectories (Figures 1G–1J and S4). That is to say that the movement of all cells is disturbed when the ICM is in contact with TNF-$\alpha$, which results in a correlation coefficient of ~0.4 (Figures 1P and 1Q). It is plausible that TNF-$\alpha$ stimulation induces temporary disassembly in the cell-cell and cell-ECM connections (Wójciak-Stothard et al., 1998), which results in decreased local stress in the connective actin layer, and thus the contractile actions coordinating with periodic TNF-$\alpha$ stimulation. Most cells return to their original positions within 20–30 min, driven by the reorganization of actin networks. The deformation of the ICM as a whole entity can, therefore, reflect changes in the intra-cellular mechanical loads caused by the actin remodeling.

The intra-cellular mechanical cues can be assessed by monitoring the changes in the nuclear shape (Figures S2T–S2V) caused by the unbalanced osmotic pressure across the nuclear envelope (NE) and cytoskeleton reorganization (Kim et al., 2015). Our results demonstrate that collective behavior emerges only at 1/20 $min^{-1}$ TNF-$\alpha$ input periodicity, showing elevated fluctuation amplitude and synchronized decrease in nuclear area (Figures 1K–1N, 1O, 1P, and S4 and Video S6) and increase in height (Figure S3M). In the meantime, H2B fluorescence intensity within the nucleus increases, suggesting more densely packed chromatin fibers. After 20 to 30 min, the nucleus restores its original shape. Of note, the nuclear shape fluctuations (NSFs) do not synchronize with TNF-$\alpha$ input, showing mode hopping between 1/20 and 1/30 $min^{-1}$ (Figure S4A), which is considerably quicker than the nuclear deformation caused by cell-cell collision (i.e., ~2 h) (Figures S2F and S2G). The amplitude of NSF is also considerably higher at 1/20 $min^{-1}$ than that of the SA cells and those stimulated by 1/60 and 1/90 $min^{-1}$ TNF-$\alpha$ inputs (Figures 1O and S5A). The deviation of NSF frequency from TNF-$\alpha$ input periodicity indicates the participation of multiple cycling processes (Canolty and Knight, 2010). These results illustrate that, upon periodic TNF-$\alpha$ stimulation, the crowded cellular environment in ICM causes distinctive morphological responses of individual cells. In contrast to the SA cells, the ordered and random morphological responses of population cells and the cytoskeleton networks in ICM causes diverse propagating mechanical cues, the coupling of which leads to complex mechanical signals. Furthermore, the nuclear shape changes in ICM upon TNF-$\alpha$ stimulation is isotropic (Figure S7C), which is morphologically different from the ones caused by the remodeling of microtubule networks shown in Figure S2G. We suspect that it is the deformation of actin filaments that alters the mechanical loads on the nucleus (Figures S2T and S2V) and causes the collective NSF.

## Dynamic cell-cell connections cause changing mechanical loads on the nucleus

The cytoskeleton reorganization in response to TNF-$\alpha$ stimulation, which actively regulates the nuclear shape, is evaluated by monitoring the remodeling of microtubule networks and the deformation of actin filaments. The remodeling of individual cells' microtubule networks was assessed by reconstructing their 3D volume via confocal z stack imaging (Figure S5B). We observed that the microtubule volume of SA cells decreases down to ~80% of the initial value, when first in contact with TNF-$\alpha$ (Figure S5C). In contrast, no obvious change was observed in the ICM. The microtubules of SA cells regain their original volume within ~1 h (Figure S5D). The remodeling of microtubule networks during periodic TNF-$\alpha$ stimulation shows no

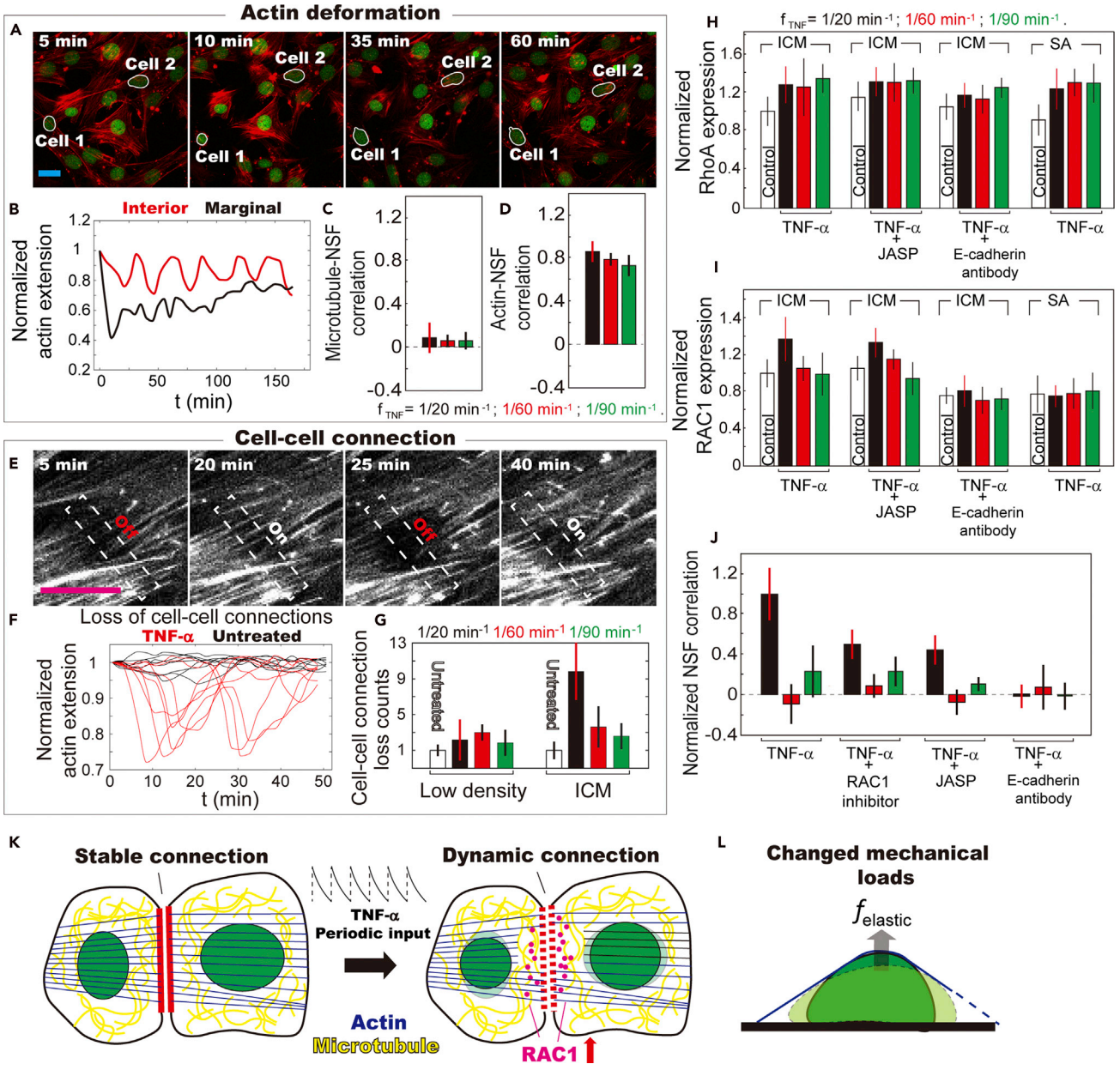


**Figure 2. Active remodeling of cytoskeleton networks and RAC1-mediated dynamic cell-cell connections lead to collective NSF**

(A) Representative fluorescent images of ICM during periodic TNF-α stimulation show that shape transition of the nuclear (green) and actin deformation (red) are more dramatic at the marginal region. Scale bar represents 20 μm.

(B) Averaged extension of actin filaments at different time points reveals that actin deformation differs at the marginal and interior area. The variations in the average actin extension were normalized by the initial value (i.e., at 0 min).

(C) Cross-correlation analysis between variations in the volume of microtubule networks and NSF illustrates that remodeling of microtubule networks has trivial effects on nuclear shape. The error bars represent standard deviation of the correlation coefficients between individual cell's microtubule remodeling and NSF.

(D) Cross-correlation analysis between variations in actin extension and NSF reveals that actin deformation regulates nuclear shape. The error bars represent standard deviation of the correlation coefficients between changes in individual cell's actin extension remodeling and NSF.

(E) Representative fluorescent images of the actin filaments at cell-cell connections during periodic TNF-α stimulation show variations in the fluorescence intensity. Scale bar represents 20 μm.

(F) Traces of the fluorescence intensity at the cell-cell connections demonstrate that the variations are more obvious with TNF-α stimulation. The variations in the average actin extension were normalized by the initial value (i.e., at 0 min).

**Figure 2. *Continued***

(G) Counts of the events with fluctuation amplitude of fluorescence intensity at cell-cell connections more than 10% show more frequent loss of cell-cell contacts with TNF-$\alpha$ stimulation. The error bars represent standard deviation of cell-cell connection loss counts among low density cells and in ICM.

(H and I) Expression level of RhoA (H) and RAC1 (I) mRNA detected by RT-PCR and expressed as fold-change. For the data presented in (H) and (I), minimum five independent experiments were performed for each data point. The expression level of both proteins was normalized by the value of control samples, i.e., the untreated ICM. The error bars represent standard deviation of protein expression level in five independent experiments at each condition.

(J) Cross-correlation analysis of the NSF of neighboring cells reveals that the collective cellular responses are disrupted by drugs regulating cell-cell connections. Correlation coefficients obtained under different conditions were normalized to the control sample, i.e., ICM treated by 1/20 $min^{-1}$ TNF-$\alpha$. The error bars represent standard deviation of the NSF correlation coefficients among population cells.

(K) Schematic shows that entrainment in the Rho-associated signaling pathways leads to an elevated RAC1 expression level, which facilitates transition to more dynamic cell-cell connections.

(L) Schematic shows that deformation of actin filaments leads to changing mechanical loads on the nucleus.

evidence of coordination among population cells in ICM (Figures 2C, S5D and supplementary information) and does not coordinate with the nuclear shape changes (i.e., the NSF) (Figure 1C). We, therefore, conclude that the microtubule only has trivial contributions to the collective NSF.

The deformation of actin filaments upon periodic TNF-$\alpha$ stimulation was evaluated by measuring the extension of single actin filaments in individual cells, the average value of which reflects changing mechanical loads on the nucleus (Figures S5E and S5F). The addition of TNF-$\alpha$ induces drastic contractile actions of actin filaments (Figure 2A and Video S7), in contrast to the case in microtubule. Cells located at the marginal region of the ICM (e.g., cell 1) show a drastic decrease in the nuclear area as compared with the ones in the interior area (e.g., cell 2) (Figure 2A). Simultaneously, the extension of actin filaments of cell 1 decreases by ~40% (Figure 2B). The actin deformation becomes less obvious with repeated TNF-$\alpha$ stimulation, during which time cell 1 gradually regains its original volume. In contrast, cell 2, which locates in the interior region of the ICM, responds to dynamic TNF-$\alpha$ stimulation in an ordered manner. The variations in the averaged actin extension remains at a fluctuation amplitude of ~20% (Figure 2B) at 1/20 $min^{-1}$ TNF-$\alpha$ input frequency and coordinates well with the NSF at all conditions (Figure 2D). These results suggest that actin deformation is the key regulator for the nuclear shape changes, and cells in the ICM adopt a different strategy from the SA cells in response to dynamic TNF-$\alpha$ stimulation.

Shivashankar et al. discovered that TNF-$\alpha$ stimulation causes actin depolymerization (Mitra, 2017). The disappearance of the actin cap leads to decreased compressive forces on the nucleus and induces nuclear shape changes, which happens within tens of minutes. We did not observe clear fragmentation of the actin filament. Instead, by monitoring the variations of fluorescent intensity at the cell-cell connections, we found that the occurrence of dynamic loss and re-establishment of cell-cell contacts increases considerably with 1/20 $min^{-1}$ TNF-$\alpha$ stimulation, as compared with other TNF-$\alpha$ input frequencies and the control samples (Figures 2E–2G). We then measured the gene expression level of two members of the Rho family, i.e., RhoA and RAC1, which was reported to regulate stable and dynamic cell-cell connections, respectively (Nguyen et al., 2018). Our results demonstrate that the expression level of RhoA exhibits equivalent increment by tuning TNF-$\alpha$ input frequencies (Figure 2H). In other words, 1/20 $min^{-1}$ TNF-$\alpha$ stimulation brings no observable effect to the RhoA signaling cascade. In contrast, RAC1 expression increases only at 1/20 $min^{-1}$ TNF-$\alpha$ input frequency (Figure 2I). The elevated expression of RAC1 at a defined TNF-$\alpha$ input frequency is similar to the entrainment in the signaling cascade (Kellogg and Tay, 2015), which is brought up by Tay, etc. to interpret coordinated and enlarged signaling activities of population cells. Therefore, we suggest that dynamic TNF-$\alpha$ stimulation activates and entrains the Rho-associated signaling pathways, leading to elevated expression of RAC1, which promotes the transition from mature to dynamic cell-cell connections (Figure 2K). As the loss of cell-cell contacts leads to changes in the extension of actin filaments and thus the mechanical loads on the nucleus (Figure 2L), the intracellular mechanical cues then cause the collective NSF shown in Figure 1K.

The hypothesis is further verified by introducing RAC1 inhibitor, Jasplakinolide (JASP), and E-cadherin antibody to the ICM. The addition of RAC1 inhibitor disrupts the collective movement of actin filaments (Figure S5G), but the collective NSF remains unaffected (Figure 2J), verifying the crucial role of RAC1. As JASP is a potent inducer of actin polymerization and known to stabilize cell-cell connections (Li et al., 2020; Holzinger, 2009), the disruption of collective NSF by JASP indicates the transition from mature to dynamic cell-cell connections as an essential linker (Figures 2J and S5G). Pretreatment of fibroblasts with E-cadherin antibody inhibits the formation of ICM and disrupts all the collective activities (Figures 2J, S5G, and S6). Possibly, when cell-cell connections are stabilized via linkers including E-cadherin, increased actin tensile

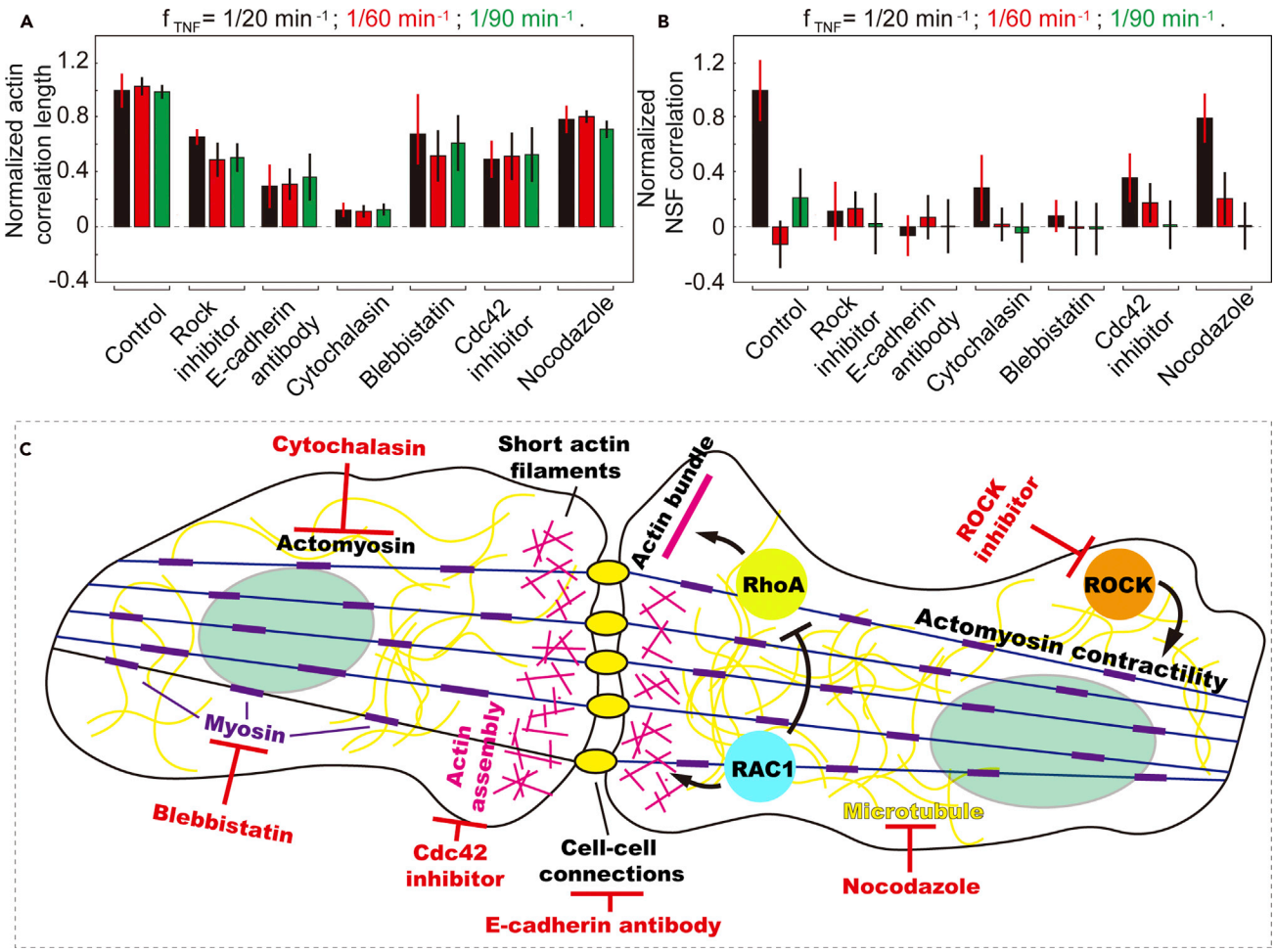


**Figure 3. Dynamic cell-cell connections and actin contractility both play crucial roles in regulating collective morphological responses in the ICM**

(A) Particle image velocimetry and correlation length analysis of actin filaments in the ICM reveal that the collective movement is disrupted by drugs targeting cell-cell connections. The correlation lengths obtained under different conditions were normalized by value of the control samples, i.e., ICM treated by only 1/20 $min^{-1}$ TNF-$\alpha$. The error bars represent standard deviation of the correlation length of actin filaments in five independent experiments.

(B) The collective NSF is disrupted by drugs targeting cell-cell connections and actin contractility but not the microtubule networks. The correlation coefficients obtained under different conditions were normalized by value of the control samples, i.e., ICM treated by only 1/20 $min^{-1}$ TNF-$\alpha$. The error bars represent standard deviation of the correlation coefficients of population cells' NSF in five independent experiments.

(C) Schematic shows that the collective NSF is regulated by deformation of actin filaments and dynamic cell-cell connections.

stress leads to stronger compressive forces on the nucleus, which is reflected by the decreased height of the nucleus in the ICM as compared with the SA cells (Figures S5H–S5J). The complete loss or stabilization of cell-cell adhesions leads to diminished variation amplitude of the mechanical load on the nucleus, and thus the lack of changes in the nuclear shape upon periodic TNF-$\alpha$ stimulation.

## Contractility of actin filaments is essential for the collective NSF

As the source of the dynamically changing mechanical forces on the nucleus, the contractility of actin filaments is of crucial importance to the collective morphological responses. To identify the crucial linkers associated with actin contractility, we introduced several drugs to the ICM and monitored the morphological responses of population cells to the dynamic TNF-$\alpha$ stimulation, including Rho-associated protein kinase (ROCK) inhibitor Y-27632, which plays central roles in mechano-transduction (Yang, 2017) and cytoskeleton reorganization (Amano et al., 2010); cytochalasin, which is reported to depolymerize actin filaments (Casella et al., 1981); Blebbistatin, which blocks myosin II activities (Kovács et al., 2004); Cdc42 inhibitor (ML-141), which disrupts actin polymerization and assembly (Hong, 2013); and Nocodazole, which depolymerizes microtubules (Figure 3) (Xu et al., 2002). We observed that the addition of ROCK inhibitor

Y-27632 disrupted the collective morphological responses in the ICM, which emerge at 1/20 $min^{-1}$ TNF-$\alpha$ input frequency, but not the collective movement (Figures 3A and 3B). Both the collective movement and morphological responses of ICM were disrupted by cytochalasin, Cdc42 inhibitor ML-141, and Blebbistatin. In contrast, Nocodazole brings no effect to the collective activities in ICM.

Taken together, these results identify several essential factors to achieve collective NSF, i.e., the cell-cell connections and the contractility and integrity of actin filaments (Figure 3C). Conceivably, during ICM formation, stretching of actin filaments leads to increased tensile stress and forces on cell-cell connections. In the untreated ICM, the linkage between neighboring cells is stabilized enough, through the formation of long actin bundles, to maintain its integrity (Zhang, 2005; Amano, 1997), whereas with 1/20 $min^{-1}$ TNF-$\alpha$ stimulation, one or multiple Rho-associated signaling pathways get activated and entrained, leading to elevated RAC1 expression level, which destabilizes E-cadherin-mediated cell-cell adhesion (Hage et al., 2009; Burridge and Wennerberg, 2004) and transits actin bundles to short filaments (Jiang et al., 2006). Consequently, cell-cell connections become more dynamic. The temporary loss and re-establishment of actin filaments with linkers (e.g., E-cadherin) lead to varying mechanical loads on the nucleus, and thus the collective NSF.

### Signaling responses of ICM under periodic TNF-$\alpha$ stimulation

The interplay between the dynamic mechanical cues caused by cytoskeleton reorganization and TNF-$\alpha$-activated signaling cascade is investigated by monitoring the transcription factor NF-$\kappa$B oscillation through the NE (Figures 4A–4D and S7A–S7C). We observed that, besides the natural frequency of NF-$\kappa$B signaling cascade (i.e., 90 $min^{-1}$) (Tay et al., 2010), NF-$\kappa$B dynamics get entrained in the ICM at 1/20 $min^{-1}$ TNF-$\alpha$ input, showing apparently stronger and more coordinated morphological and signaling response than the SA cells (Figures 4E–4H and S7A–S7G). Unlike other oscillators like ERK, Crz1, and NFAT4 (Albeck et al., 2013; Berridge et al., 2003; Cai et al., 2008; Dolmetsch et al., 1998), whose oscillation frequencies depend on the input signal concentration, NF-κB oscillation frequency (90–100 min peak-to-peak interval) is unchanged across a wide range of input concentrations (Longo et al., 2013; Tay et al., 2010; Turner et al., 2010). According to these results, the 1/20 $min^{-1}$ TNF-α stimulation is sufficiently mismatched from the 90-min NF-κB natural periodicity to induce a disrupted, non-entrained NF-κB response in most cells, which is consistent with our observations on the SA cells (Figure S7A, S7D, and S7E). We, therefore, suggest that cell-cell interaction in the crowded environment of the ICM affects cellular responses, i.e., NF-κB oscillation.

In the meantime, the number of activated cells upon repeated TNF-$\alpha$ stimulation increases in the ICM as well (Figures S7H and S7I). For example, the fraction of active cells is ~20% higher in the ICM than in the SA ones when the input TNF-$\alpha$ concentration is 0.08 ng/mL. Of note, with 1/20 $min^{-1}$ TNF-$\alpha$ stimulation, the NF-$\kappa$B shows an oscillating frequency of ~1/26 $min^{-1}$, which coordinates with the collective action of NSF but deviates from the TNF-$\alpha$ input periodicity (Figures S7A and S7B). As fibroblasts in the ICM are genetically identical with those of the SA cells, these results suggest that the intracellular mechanical cues caused by cytoskeleton reorganization in the ICM affect the proceeding of biochemical signaling cascade.

The addition of ROCK inhibitor, E-cadherin antibody, cytochalasin, Blebbistatin, Cdc42 inhibitor (ML-141), and JASP, which disrupt the collective NSF at 20 $min^{-1}$ TNF-$\alpha$ input, disrupted the collective signaling responses of population cells in the ICM as well (Figure 4I). In contrast, the entrained NF-$\kappa$B oscillation at the natural frequency of 1/90 $min^{-1}$ is not affected. These results show that at 1/90 $min^{-1}$ TNF-$\alpha$ input frequency, the mechanical cues delivered to the nucleus are mostly random and relatively small (Figures 1M, 1O, and 1P). The entrained cycling of NF-$\kappa$B signaling cascade is, therefore, not affected, whereas at 1/20 $min^{-1}$ TNF-$\alpha$ input, where the intracellular mechanical forces are maximized, the collective NSF facilitates NF-$\kappa$B oscillation at a frequency far beyond the natural value, i.e., from 90 to 20 $min^{-1}$.

### Stand-alone cells on chip: mechanical cues at the cell-ECM interface enhance NF-κB dynamics

To investigate the regulatory effects of chemically induced intracellular mechanical cues, we designed a microfluidic device in which forces mimicking those in ICM can be directly applied on SA cells (Figures 5A, S8A, and S8B). In the collagen matrix, investigation on SA cells, instead of population cells, excludes the effect of cell-cell communication through chemical information exchange (Figure 5B) and uncontrollable mechanical cues caused by the movement neighboring cells (Video S8). The programmed on-off of four control channels, which are connected to the stretchable PDMS membrane underneath the collagen matrix, causes remodeling (Figures S8C–S8F and Video S9) and thus induces dynamic mechanical cues to SA cells (Figures 5B and S8G–S8I, and Video S10). The amplitude and types of induced morphological

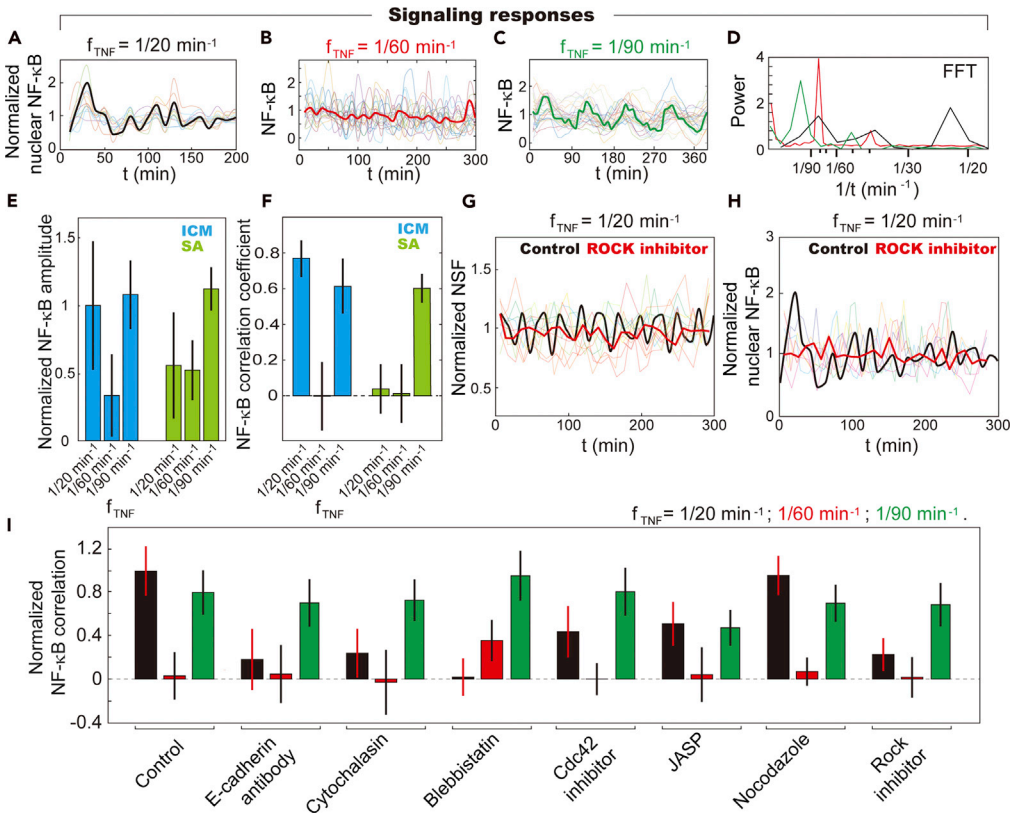


**Figure 4. Collective signaling response of population cells in ICM upon periodic TNF-$\alpha$ stimulation**

(A–C) NF-$\kappa$B dynamics of individual cells in ICM upon periodic TNF-$\alpha$ stimulation. NF-κB traces were normalized by the average value.

(D) Fast Fourier transform (FFT) shows dominant oscillation frequency close to NSF. In (A)-(C), the translucent lines are the traces of individual cells and the solid lines reflect the averaged value of single cells traces.

(E) NF-$\kappa$B oscillation amplitude is maximized at 1/90 min$^{-1}$, when getting entrained, and greatly enhanced in the ICM in response to 1/20 min$^{-1}$ TNF-$\alpha$ stimulation as compared with SA cells. The NF-κB oscillation amplitude of individual cells under different conditions was normalized by value of the control samples, i.e., ICM treated by only 1/20 min$^{-1}$ TNF-α. The error bars represent standard deviation of population cell's nuclear NF-κB fluctuation amplitude.

(F) Cross-correlation analysis of the signaling responses of population cells in the ICM reveals that the collective behavior is most obvious in NF-$\kappa$B dynamics when stimulated by 1/20 and 1/90 min$^{-1}$ TNF-$\alpha$ in ICM, and only at 1/90 min$^{-1}$ TNF-$\alpha$ for SA cells. The error bars represent standard deviation of the correlation coefficients of population cells' NF-κB oscillation through NE.

(G and H) NF-$\kappa$B and NSF traces of single fibroblasts in ICM treated with ROCK inhibitor, which is followed by 1/20 min$^{-1}$ TNF-$\alpha$ stimulation. The NSF and NF-κB traces were normalized by their average values. In (G)-(H), the translucent lines are the traces of individual cells being treated by ROCK inhibitor and the solid lines reflect the averaged value of single cells traces. It is demonstrated that the application of ROCK inhibitor disrupts the collective activities of the ICM in NSF and NF-$\kappa$B dynamics shown in Figures 1K and 4A.

(I) The collective signaling responses were disrupted by drugs, which disrupt collective NSF. The collective cellular responses at 1/90 min$^{-1}$ were unaffected. The NF-κB correlation coefficient of neighboring cells under different conditions were normalized by value of the control samples, i.e., ICM treated by only 1/20 min$^{-1}$ TNF-α. The error bars represent standard deviation of the correlation coefficients of NF-κB oscillation under different experimental conditions.

fluctuation depend on the inflating pressure as well as the location of the cells with respect to the PDMS membrane, i.e., longitudinal stretching (elongated cell morphology), lateral stretching (increased cell surface area), and compression (decreased area) (Figures S8G–S8I). Of note, the induced mechanical cues at the cell-ECM interface bring no observable changes in the nuclear shape (Figure 5C).

In the platform, TNF-$\alpha$ inputs of 1/20, 1/60, and 1/90 min$^{-1}$ periodicities and dynamic collagen remodeling of 1/20 to 1/90 min$^{-1}$ frequencies were then simultaneously introduced to SA cells. We observed that NF-$\kappa$B oscillation in responses to 1/20 min$^{-1}$ TNF-$\alpha$ stimulation is only slightly enhanced under certain

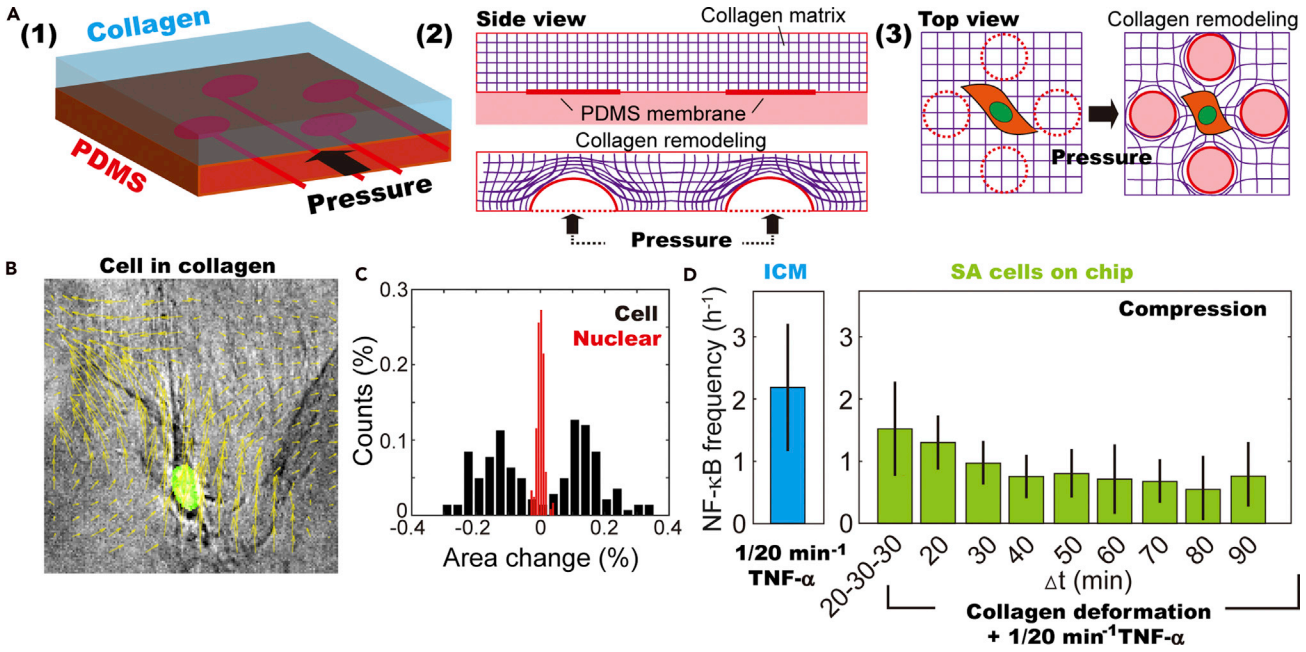


**Figure 5. Modeling the dynamic mechanical cues at cell-ECM interfaces using a customized microfluidic device**

(A) Sketch of the collagen remodeling caused by repeated pressurization and relaxation of the underlying PDMS membrane, which then delivers dynamic mechanical cues to the SA cells.

(B) Remodeling of the collagen matrix leads to cell shape transition (phase contrast). The nuclear shape (green) remains mostly unaffected.

(C) Distribution of nuclear and cell area changes suggests that remodeling of the collagen matrix brings no obvious effects on the nuclear shape.

(D) Subjected to repeated collagen remodeling at frequencies ranging from 1/20 to 1/90 $min^{-1}$, 1/20 $min^{-1}$ TNF-$\alpha$ is insufficient to achieve NF-$\kappa$B oscillation frequency comparable with ICM. NF-$\kappa$B dynamics is, however, enhanced, when the frequency of induced collagen remodeling is 1/20 $min^{-1}$ or mode hopping between 1/20 and 1/30 $min^{-1}$. The error bars represent standard deviation of population cells' NF-$\kappa$B oscillation frequency through NE.

conditions, i.e., when SA cells are repeatedly compressed at 1/20 $min^{-1}$ frequency or mode hopping between 1/20 and 1/30 $min^{-1}$ (Figures 5D, S8J, and S8K). Even though NF-$\kappa$B oscillation frequency of few SA cells reaches 1/30 $min^{-1}$, the enhanced and coordinated NF-$\kappa$B dynamics comparable with the ICM is not yet accomplished. The failure in reconstituting the intracellular morphological and signaling responses in the ICM suggests that the enhancement in NF-$\kappa$B dynamics shown in Figure 4A is closely associated with the collective NSF caused by deformation of actin filaments but not the remodeling of microtubule networks during cell-cell collision (Figure S2K).

## Stand-alone cells on chip: intracellular dynamic mechanical cues facilitate NF-κB dynamics

To verify our hypothesis that actin filaments rather than microtubules regulate signaling activities, actin deformation was induced by directly plating fibroblasts on the stretchable PDMS membrane (Figures S9A–S9G). Stretching or shrinking of cell adhering PDMS membrane surface alters cell adhesion area and consequently translocates the focal adhesions connected to actin filaments (Geiger et al., 2009; Goldyn et al., 2009), which alters the stress in actin filaments and induces NSF (Figures S9A and S9E) (Vishavkarma et al., 2014). We demonstrated that the induced NSF is morphologically similar to the individual cells in the ICM upon TNF-$\alpha$ stimulation. For example, if cells are initially plated on the inflated membrane at t = 0 min (i.e., initially), the adhesion area will rapidly decrease when the pressure is released at t = 10 min (Figure S9F). The SA cells were compressed at this moment with maximized nuclear height, and gradually restore their original conformation within ~10 min (Figures S9F and S9G). It is intriguing that we observed that the responsiveness of fibroblasts changes during induced NSF (Figures S9H–S9J). The SA cells are more responsive to TNF-$\alpha$ stimulation when being compressed, and the fraction of active cells decreases as cells go back to their original shape. Studies by Agnès, et al. revealed that the signaling cascades can be regulated by variances in cell and nuclear shape, which causes cytoskeleton reorganization and unbalances osmotic pressure across the NE(Miermont et al., 2013). Apparently, when the collective NSF emerges at 1/20 $min^{-1}$ TNF-$\alpha$ input frequency, mechanical loads on the nucleus are repeatedly decreased, forcing population cells in the ICM to a more responsive state (Figure S9I).

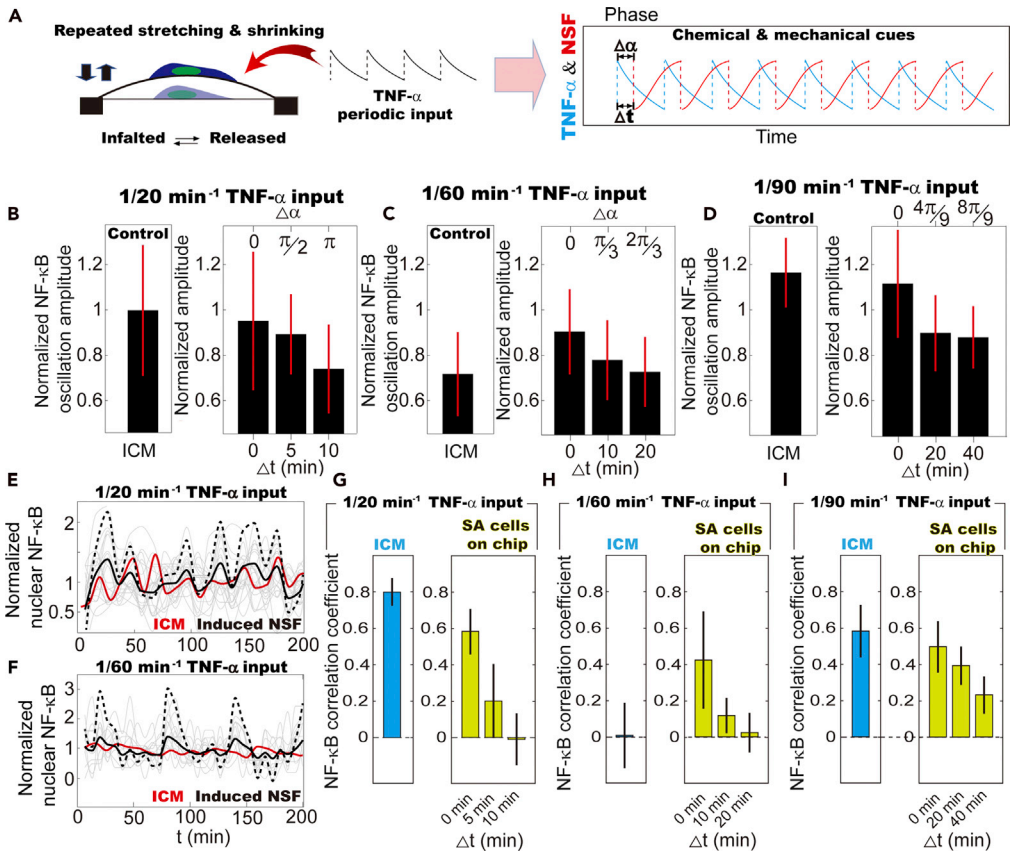


**Figure 6. Modeling intracellular mechanical cues caused by actin deformation in the ICM: the effect of dynamic mechanical cues on NF-κB oscillation of SA cells**

(A) NSF and TNF-α inputs are simultaneously introduced to SA cells using a customized microfluidic device. The time (Δt) and phase (Δα) difference between minima of the nuclear area (red) and maxima of TNF-α concentration models the phase mismatching between mechanical and chemical cues in the ICM.

(B–D) Synergy between NSF and TNF-α inputs induces elevated NF-κB oscillation amplitude among SA cells, which is comparable with or even higher than the ones in the ICM. The NF-κB oscillation amplitudes under different conditions were normalized by value of the control samples, i.e., ICM treated by only 1/20 $min^{-1}$ TNF-α. The error bars represent standard deviation of population cell's nuclear NF-κB fluctuation amplitude in five independent experiments.

(E and F) Synergy between NSF and TNF-α inputs induces collective NF-κB oscillation activities coordinating with TNF-α periodicity. NF-κB dynamics averaged among all cells with induced NSF (black lines) shows higher amplitude as compared with the ones in the ICM (red lines) when being stimulated by 1/60 $min^{-1}$oscillatory TNF-α input. The values are comparable in the ICM and on-chip in response to 1/20 $min^{-1}$ oscillatory TNF-α input. The dashed lines are the enlarged view of the black lines. The translucent lines are the traces of individual cells with induced NSF on chip. Nuclear NF-κB traces were normalized by their average values.

(G–I) Cross-correlation analysis of the signaling responses of population cells in the ICM in response to 1/20, 1/60, and 1/90 $min^{-1}$ TNF-α input reveals that collective signaling activities emerge as long as the induced NSF coordinates with the dynamic chemical inputs. The error bars represent standard deviation of the correlation coefficients of population cells' NF-κB oscillation through NE in five independent experiments.

We then repeatedly stretched or shrunk the cell adhesion surface and simultaneously introduced periodic TNF-α stimulations to the SA cells (Figure 6A). During 1/20 $min^{-1}$ periodic TNF-α stimulation, phase matching between the induced NSF and TNF-α to SA cells ($\Delta t = 0$, $\Delta\phi = 0$) leads to increased NF-κB oscillation amplitude comparable with the signaling responses in the ICM (Figure 6B). An enlarged phase difference ($\Delta t$ = 5 and 10 min; $\Delta\phi = \pi/3$ and $2\pi/3$) causes decreased nuclear NF-κB level. In the meantime, the otherwise random NF-κB dynamics of SA cells, as shown in Figure S7E, get more coordinated with synergized NSF and TNF-α input, showing a shared frequency of ~1/20 $min^{-1}$ (Figures 6E and 6G). A similar effect was observed with 1/60 and 1/90 $min^{-1}$ TNF-α inputs as well (Figures 6C, 6D, 6F, 6H, and 6I). We thus conclude that the collective NSF in the ICM facilitates NF-κB signaling activities, in which the phase

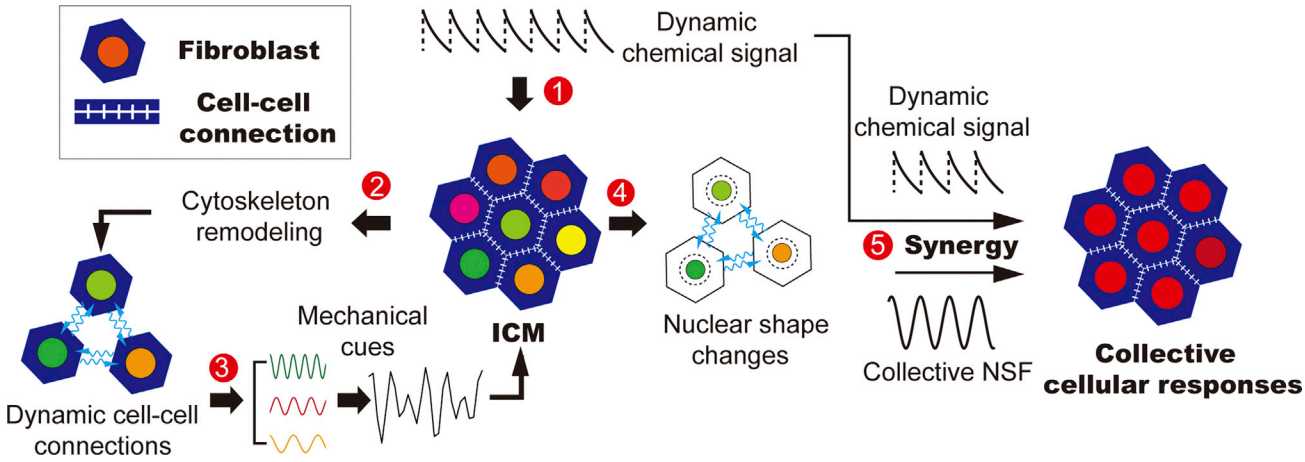


**Figure 7. Schematic shows the feedback loop, in which dynamic intracellular mechanical cues caused by active cytoskeleton reorganization synergize with the chemical signal to facilitate collective cellular responses**

In the feedback loop, dynamic chemical signals are converted into mechanical cues via RAC1-mediated transition from mature into dynamic cell-cell connections.

matching between dynamic chemical inputs and NSF (i.e., the active cytoskeleton reorganization) leads to coordinated NF-$\kappa$B oscillation more frequently than the natural frequency of 1/90 $min^{-1}$ (Tay et al., 2010). The entrained NF-$\kappa$B signaling at 1/90 $min^{-1}$ TNF-$\alpha$ input can be disrupted by inducing phase-mismatching NSF (Figure 6I), which further emphasizes the importance of synergy between intracellular physical and chemical signals and suggests a regulatory effect of the dynamic mechanical cues.

### The feedback loop translating periodic chemical input into dynamic mechanical cues

Taken together, our results suggest a feedback loop intrinsic to the crowded cellular environment in the ICM, where dynamic mechanical cues caused by cytoskeleton remodeling facilitate collective cellular responses (Figure 7). In stages  and ②, when the periodic chemical stimulation meets the natural frequency of signaling pathways associated with cytoskeleton reorganization, the elevated expression level of regulators (e.g., RAC1) leads to changes in the cell-cell connections from stable to a more dynamic state (Jiang et al., 2006). The loss of connections diminishes the extension of actin filaments and thus alters the mechanical loads on individual nuclei. The cyclic process continues when cells in the ICM reconnect with their neighbors (stage ③). The multi-frequency NSF (i.e., mode hopping between 1/20 and 1/30 $min^{-1}$) may be caused by the participation of other dynamic signals, e.g., the TNF-$\alpha$-caused contractile action of ICM and proceeding of mechano-signaling pathways, all of which cause changing mechanical forces on the nucleus (stage ④). As the consequence of dynamic mechanical cues feeding back to the ICM, the collective NSF synergizes with the dynamic chemical input, leading to the collective cellular responses at a frequency far beyond the natural value of the signaling cascade (stage ⑤).

## CONCLUSIONS

In this study, we quantified the collective morphological and signaling responses of population cells in an ICM, which models the crowded cellular environments in the biological tissue. Using a microfluidic chip and live cell imaging system, dynamic TNF-$\alpha$ stimulations at input frequencies of 1/20, 1/60, and 1/90 $min^{-1}$ were introduced to either SA cells or the ICM. The correlation between the intracellular mechanical loads and collective signaling responses was investigated by simultaneously monitoring the cytoskeleton reorganization and NF-$\kappa$B oscillation dynamics in response to periodic TNF-$\alpha$ stimulations.

We found that, for the SA cells, NF-$\kappa$B oscillation gets coordinated with its amplitude reaching maximum under only 1/90 $min^{-1}$ TNF-$\alpha$ stimulation, which is consistent with the reported natural frequency of NF-$\kappa$B signaling cascade, whereas in the crowded environment of the ICM, NF-$\kappa$B oscillation gets maximum coordination at both 1/90 and 1/20 $min^{-1}$ of TNF-$\alpha$ input frequencies. In the meantime, at the particular TNF-$\alpha$ input frequency of 1/20 $min^{-1}$, the RAC1 expression level is unexpectedly elevated. This leads to enhanced transition from mature to dynamic cell-cell connections and more frequent on-off of cell-cell

contacts, which cause a decrease in the overall extension of actin filaments in the cell. Subsequently, the properties (i.e., characteristic frequency and amplitude) of intracellular mechanical cues are altered, leading to an amplified morphological and signaling response of the ICM to 1/20 $min^{-1}$ TNF-$\alpha$ stimulation. These results indicate an intracellular mechanism facilitating the collective signaling responses of population cells in the ICM, in which chemical stimulations are translated into dynamic mechanical cues through RAC1-mediated active cytoskeleton reorganization.

The intracellular mechanism determining the collective morphological and signaling responses was further studied by isolating SA cells in a customized microfluidic device, which can induce remodeling of cytoskeleton networks and independently generate dynamic chemical signals. Excluding the effect of cell-cell communication, we demonstrate that, regardless of the input frequencies of mechanical and chemical stimulations, responses of SA cells on par with the ICM can be accomplished as long as the induced dynamic cytoskeleton remodeling phase matches with the TNF-$\alpha$ stimulation periodicities. This supports our finding that NF-$\kappa$B dynamics in ICM is only enhanced at 1/20 $min^{-1}$ stimulation periodicity, where NSF reflecting the intracellular mechanical cues and the TNF-$\alpha$ input frequency are most coordinated. The emergence of collective morphological and signaling responses at a defined TNF-$\alpha$ input frequency of 1/20 $min^{-1}$ implies that there exists a feedback loop in the ICM, in which the periodic TNF-$\alpha$ stimulation leads to entrainment in the RAC1-associated signaling pathways and cytoskeleton reorganization. Subsequently, the changing mechanical loads on the nucleus cause the collective NSF, which synergizes with the dynamic TNF-$\alpha$ stimulation and facilitates collective cellular responses.

Our findings reveal a novel strategy that allows the biological tissue to generate phase-locked responses to acute inflammatory signaling far beyond its natural frequency. Beside its biological significance, the regulatory effects of dynamic mechanical cues on collective cellular responses suggest new therapeutic strategies, in which dynamic mechanical signals can be induced by acoustic or magnetic field to minimize the cell-to-cell variability *in vivo* and get a coherent downstream response. Furthermore, our studies demonstrated the capacities of the presented microfluidic system in generating phase mismatching between the dynamic chemical and physical signals at milliseconds accuracy, which allows us to systematically investigate the importance of synergy between various environmental cues in regulating collective cellular responses.

### Limitations of this study

Regarding the dynamic mechanical cues, which regulate intracellular signaling activities, the limitation of this study is that we have not yet quantified these forces. One of the remaining questions is how nucleus as the mechanosensor distinguishes diverse mechanical cues. For example, nuclear deformation was often observed during cell-cell collision. Would the transduced mechanical forces affect cellular responses?

### Resource availability

#### *Lead contact*

Further information and requests for resources and reagents should be directed to and will be fulfilled by the lead contact, Ce Zhang (zhangce.univ@gmail.com). ***Materials availability*** This study did not generate new unique reagents.

#### *Data and code availability*

All relevant data are available from the authors upon request.

## METHODS

All methods can be found in the accompanying transparent methods supplemental file.

## SUPPLEMENTAL INFORMATION

Supplemental information can be found online at https://doi.org/10.1016/j.isci.2021.102396.

## ACKNOWLEDGMENTS

This study is supported by National Natural Science Foundation of China (NSFC: 51924807 and 51927804).

## AUTHORS CONTRIBUTIONS

C.Z. and B.C. designed and conducted the experimental study. W.Z., D.S., X.F., J.B., and G.J. designed and performed statistical analysis. All authors contributed to the writing of the manuscript.

## DECLARATION OF INTERESTS

The authors declare that they have no competing interests. The two-level culture chamber described in this article has been patented by the University of Chicago (Pub. No: WO/2018/213282, International Application No. PCT/US2018/032727).

Received: November 17, 2020
Revised: February 11, 2021
Accepted: April 2, 2021
Published: May 21, 2021

## REFERENCES

Amano, M. (1997). Formation of actin stress fibers and focal adhesions enhanced by Rho-kinase. Science *275*, 1308–1311.

Amano, M., Nakayama, M., and Kaibuchi, K. (2010). Rho-kinase/ROCK: a key regulator of the cytoskeleton and cell polarity. Cytoskeleton *67*, 545–554.

Albeck, John G., Mills, Gordon B., and Cell, Joan S.B.J.M. (2013). Frequency-Modulated pulses of ERK activity transmit quantitative proliferation signal. Mol. Cell *49*, 249–261.

Asnacios, A., and Hamant, O. (2012). The mechanics behind cell polarity. Trends Cell Biol. *22*, 584–591.

Berridge, M.J., Bootman, M.D., and Roderick, H.L. (2003). Calcium signalling: dynamics, homeostasis and remodelling. Nat. Rev. Mol. Cell Biol. *4*, 517–529.

Box, K., Joyce, B.W., and Devenport, D. (2019). Epithelial geometry regulates spindle orientation and progenitor fate during formation of the mammalian epidermis. Elife Sci. *8*, e47102.

Burridge, K., and Wennerberg, K. (2004). Rho and rac take center stage. Cell *116*, 167–179.

Cai, L., Dalal, C.K., and Elowitz, M.B. (2008). Frequency-modulated nuclear localization bursts coordinate gene regulation. Nature *455*, 485–490.

Canolty, R.T., and Knight, R.T. (2010). The functional role of cross-frequency coupling. Trends Cogn. Sci. *14*, 506–515.

Casella, J.F., Flanagan, M.D., and Lin, S. (1981). Cytochalasin D inhibits actin polymerization and induces depolymerization of actin filaments formed during platelet shape change. Nature *293*, 302–305.

Copos, C., and Mogilner, A. (2020). A hybrid stochastic-deterministic mechanochemical model of cell polarization. Mol. Biol. Cell *31*, 1637–1649.

Dolmetsch, Ricardo, Keli, E., and Lewis, Richard (1998). Calcium oscillations increase the efficiency and specificity of gene expression. Nature *392*, 933.

Floris, Bosveld, Isabelle, Bonnet, Boris, Guirao, Sham, Tlili, Zhimin, and Wang. (2012). Mechanical control of morphogenesis by fat dachsous four-jointed planar cell polarity pathway. Science *336*, 724–727.

Frangogiannis, N.G. (2016). Fibroblast—extracellular matrix interactions in tissue fibrosis. Curr. Pathobiol. Rep. *4*, 11–18.

Friedl, P., and Wolf, K. (2003). Tumour-cell invasion and migration: diversity and escape mechanisms. Nat. Rev. Cancer *3*, 362–374.

Geiger, B., Spatz, J.P., and Bershadsky, A.D. (2009). Environmental sensing through focal adhesions. Nat. Rev. Mol. Cell Biol. *10*, 21–33.

Goldyn, A.M., Rioja, B.A., Spatz, J.P., Ballestrem, C., and Kemkemer, R. (2009). Force-induced cell polarisation is linked to RhoA-driven microtubule-independent focal-adhesion sliding. J. Cell Sci. *122*, 3644–3651.

Gudipaty, S.A., Lindblom, J., Loftus, P.D., Redd, M.J., Edes, K., Davey, C.F., Krishnegowda, V., and Rosenblatt, J. (2017). Mechanical stretch triggers rapid epithelial cell division through Piezo1. Nature *543*, 118–121.

Hage, B., Meinel, K., Baum, I., Giehl, K., and Menke, A. (2009). Rac1 activation inhibits E-cadherin-mediated adherens junctions via binding to IQGAP1 in pancreatic carcinoma cells. Cell Commun. Signal. *7*, 23.

Harris, A.R. (2012). Characterizing the mechanics of cultured cell monolayers. Proc. Natl. Acad. Sci. U S A *109*, 16449–16454.

He, L., Si, G., Huang, J., Samuel, A.D.T., and Perrimon, N.J.N. (2018). Mechanical regulation of stem cell differentiation through stretch-activated Piezo channel. Nature *555*, 103–106.

Holzinger, A. (2009). Jasplakinolide: an actin-specific reagent that promotes actin polymerization. Methods Mol. Biol. *586*, 71–87.

Hong, L. (2013). Characterization of a Cdc42 protein inhibitor and its use as a molecular probe. J. Biol. Chem. *288*, 8531–8543.

Jiang, H., Sha, S.-H., and Schacht, J. (2006). Rac/Rho pathway regulates actin depolymerization induced by aminoglycoside antibiotics. J. Neurosci. Res. *83*, 1544–1551.

Kellogg, R.A., and Tay, S. (2015). Noise facilitates transcriptional control under dynamic inputs. Cell *160*, 381–392.

Khalilgharibi, N., Fouchard, J., Asadipour, N., Barrientos, R., Duda, M., Bonfanti, A., Yonis, A., Harris, A., Mosaffa, P., and Fujita, Y. (2019). Stress relaxation in epithelial monolayers is controlled by the actomyosin cortex. Nat. Phys. *15*, 839–847.

Kim, D.H., Li, B., Si, F., Phillip, J.M., Wirtz, D., and Sun, S.X. (2015). Volume regulation and shape bifurcation in the cell nucleus. J. Cell Sci. *128*, 3375–3385.

Kovács, M., Tóth, J., Hetényi, C., Málnási-Csizmadia, A., and Sellers, J.R. (2004). Mechanism of blebbis-tatin inhibition of myosin II. J. Biol. Chem. *279*, 35557–35563.

Lecaudey, V., and Gilmour, D. (2006). Organizing moving groups during morphogenesis. Curr. Opin. Cell Biol. *18*, 102–107.

Li, J.X.H., Tang, V.W., and Brieher, W.M. (2020). Actin protrusions push at apical junctions to maintain E-cadherin adhesion. Proc. Natl. Acad. Sci. *117*, 432–438.

Longo, D.M., Selimkhanov, J., Kearns, J.D., Hasty, J., Hoffmann, A., Tsimring, L.S., and Shvartsman, S. (2013). Dual delayed feedback provides sensitivity and robustness to the NF-κB signaling module. PLoS Comput. Biol. *9*, e1003112.

Miermont, A., Waharte, F., Hu, S., McClean, M.N., Bottani, S., Leon, S., and Hersen, P. (2013). Severe osmotic compression triggers a slowdown of

intracellular signaling, which can be explained by molecular crowding. Proc. Natl. Acad. Sci. *110*, 5725–5730.

Mitra, A. (2017). Cell geometry dictates TNFα-induced genome response. Proc. Natl. Acad. Sci. U S A *114*, 3882–3891.

Nguyen, L.K., Kholodenko, B.N., and Kriegsheim, A. (2018). Rac1 and RhoA: networks, loops and bistability. Small GTPases *9*, 316–321.

Pan, Y., Heemskerk, I., Ibar, C., Shraiman, B.I., and Irvine, K.D. (2016). Differential growth triggers mechanical feedback that elevates Hippo signaling. Proc. Natl. Acad. Sci. *113*, E6974–E6983.

Roure, O.D., Saez, A., Buguin, A., Austin, R.H., Chavrier, P., Silberzan, P., and Ladoux, B. (2005). Force mapping in epithelial cell migration. Proc. Natl. Acad. Sci. *102*, 2390–2395.

Sun, B., Lembong, J., Normand, V., Rogers, M., and Stone, H.A. (2012). Spatial-temporal dynamics of collective chemosensing. Proc. Natl. Acad. Sci. *109*, 7753–7758.

Tay, S., Hughey, J.J., Lee, T.K., Lipniacki, T., Quake, S.R., and Covert, M.W. (2010). Single-cell NF-κB dynamics reveal digital activation and analogue information processing. Nature *466*, 267–271.

Turner, D.A., Paszek, P., Woodcock, D.J., Nelson, D.E., and Harper, C.V. (2010). Physiological levels of TNFalpha stimulation induce stochastic dynamics of NF-kappaB responses in single living cells. J. Cell Sci. *123*, 2834–2843.

Vishavkarma, R., Raghavan, S., Kuyyamudi, C., Majumder, A., Dhawan, J., and Pullarkat, P.A. (2014). Role of actin filaments in correlating nuclear shape and cell spreading. PLoS One *9*, e107895.

Wells, R.G., and Discher, D.E. (2008). Matrix elasticity, cytoskeletal tension, and TGF-: the insoluble and soluble meet. Sci. Signal. *1*, pe13.

Wójciak-Stothard, B., Entwistle, A., Garg, R., and Ridley, A.J. (1998). Regulation of TNF-α-induced reorganization of the actin cytoskeleton and cell-cell junctions by Rho, Rac, and Cdc42 in human endothelial cells. J. Cell Physiol. *176*, 150–165.

Xu, K., Schwarz, P.M., and Ludueña, R.F. (2002). Interaction of nocodazole with tubulin isotypes. Drug Dev. Res. *55*, 91–96.

Yang, N. (2017). Cellular mechano-environment regulates the mammary circadian clock. Nat. Commun. *8*, 14287.

Zhang, C., Tu, H.L., and Jia, G. (2019). Ultra-multiplexed analysis of single-cell dynamics reveals logic rules in differentiation. Sci. Adv. *5*, eaav7959.

Zhang, J. (2005). Actin at cell-cell junctions is composed of two dynamic and functional populations. J. Cel. Sci. *118*, 5549–5562.

Zhang, J., Alisafaei, F., Nikolić, M., Nou, X.A., Kim, H., Shenoy, V.B., and Scarcelli, G. (2020). Nuclear mechanics within intact cells is regulated by cytoskeletal network and internal nanostructures. Small *16*, 1907688.

**iScience, Volume *24***

## Supplemental information

# Dynamic intracellular mechanical cues facilitate collective signaling responses

**Bingchen Che, Wei Zhao, Yanan Liu, Dan Sun, Guangyin Jing, Jintao Bai, Xiqiao Feng, and Ce Zhang**

## Transparent Methods

### 1.1 Design and Fabrication of Microfluidic Chips

We designed and fabricated the microfluidic devices for generation of dynamic chemical and mechanical cues following the standard protocol, which was reported elsewhere (*1*). Briefly, we designed our microfluidic device shown in Fig. S1, which contains 200 culture units for the maintenance and stimulation of the interconnected cell monolayer (ICM) and stand-alone (SA) cells, using AutoCAD (Autodesk Inc., San Rafael, CA, USA). Templates for control, flow and middle membrane layers are fabricated using standard UV-lithography, using SU-8 3025, SU-8 3075 (Microchem, Westborough, MA, USA) and AZ-50X (AZ Electronic Materials, Luxembourg) photoresists. To fabricate the chip, 72g of PDMS (10:1 of monomer:catalyst ratio) was mixed, de-bubbled and poured over the Trimethylchlorosilane treated patterned silicon wafer. The PDMS was then cured for 60 min at 80 ℃. Following plasma and alignment between flow, control and membrane layer, inlet holes were then punched after two-hour thermal bonding. The chip was bonded to a PDMS coated coverslip and cured for at least 24 hours at 80 ℃ before use.

The fluidic chip, which generate dynamic mechanical cues, was design using SolidWorks (Dassault Systèmes SolidWorks Corp., CA, USA). The templates for different layers were fabricated using 3D printing (CR-3040, CREALITY, China), which were smoothed using Polysher. The PDMS chip was then produced using standard soft lithography protocol as described above.

### 1.2 Chip Setup, Operation and Control

The glass slide carrying the microfluidic chip was cleaned and taped on a slide holder. Control channels were connected to miniature pneumatic solenoid valves (Festo, Switzerland) that were controlled with a custom MATLAB (MathWorks, US) through graphical user interface *(1)*. Optimal closing pressures of push-up PDMS membrane valves were determined individually for each chip, typically ranging from 25 to 30 psi for the chips produced using UV lithography and 5 to 10 psi for the 3D-printed ones. The cell culture chambers were treated with fibronectin (0.25 mg/mL; Millipore, Austria) for 3T3 fibroblast culture. The remaining coating solution was flushed off from the chip using either PBS or cell culture media. Cell culture media is pre-warmed on chip for overnight before cell loading.

### 1.3 Cell Culture and Loading

NIH 3T3 p65-/- cells were transfected with p65-dsRed and H2B-GFP for tracking and analysis of NF-κB activation and nuclear shape changes. These cells are cultured according to the established protocols (*2*). The cytoskeleton elements (i.e., actin and microtubule) were visualized by staining cells with SiR-actin kit and SiR-tubulin kit (Cytoskeleton, Inc., US). For studies on the stand-alone (SA) cells, 3T3 fibroblasts are harvested at 80% confluence with trypsin, re-suspended and loaded into chips through semi-automated loading program at cell density from $10^4$ to $10^6$ per milliliter depending on the desired cell density. To construct an interconnected cell monolayer (ICM), cells were cultured at ~100% confluency for 24 h either in 96-well plate before being transferred to the microfluidic device through connected tubing, or directly on chip before stimulation.

The environmental conditions are maintained using temperature control and incubator system (OKOLab, NA, Italy) to strictly 37 ℃ and >98% humidity and 5% $CO_2$ during the experiment, and the PDMS chip is covered with a stage top incubator connected to a humidifier and a gas exchanger.

### 1.4 Maintaining cells in the collagen matrix on chip

To produce collagen matrix on chip, 225 μL collagen solution (Millipore Sigma) at 3 mg/mL concentration was mixed with 45 μL 7.5% $NaHCO_3$ in MEM right before adding into the 100 μL cell solution. In order to maintain 3T3 fibroblasts in the collagen matrix at the single cell level, cells were suspended at $10^4$/mL density. The collagen and cell solutions were quickly mixed right before being loaded into the fluidic device, which was pretreated to 37 ℃. The collagen solidifies and traps single cells within 5 to 10 min.

### 1.5 Live-cell Fluorescence Microscopy and Data analysis

For image acquisition, Nikon Ti2-ECLIPSE microscope with an automated translational stage and a digital CMOS camera (ORCA-Flash 4.0, Hamamatsu, Japan), and Nikon A1 confocal microscope were used. The stage and image acquisition were controlled via the NIS Elements software (Nikon, Japan). Bright field and fluorescence images were acquired and analyzed using a customized MATLAB program. The algorithm extracts 2D morphological features, including outline of individual cells, surface area, nuclear area, nuclear height, actin extension, and 3D microtubule volume by 3D reconstructing the confocal z-stack images. Trajectories of the individual cells were retrieved by tracking the position of nuclear centroids, using which the distance and area between neighboring cells were quantified.

### 1.6 Isolation of mRNA and quantification via RT-PCR

To estimate the expression level of proteins associated with cell-cell connections, 3T3 fibroblasts were firstly maintained on chip at 100% confluency for 24 h to form confluent cell monolayer, or at ~ 30% for the stand-alone cells. After repeated TNF-α stimulation for 4 h, cells were collected from the fluidic chips and fully ground in 1 ml Takara RNAiso Plus Kit (Trizol) for quantification of RAC1 and RhoA mRNA level. The supernatant after centrifuging at 12,000 rpm at 4 ℃ for 5 min was extracted twice by chloroform. The sedimentation after centrifuging at 12,000 rpm at 4 ℃ for 15 min in isopropyl alcohol was resuspended in 75% alcohol. Total RNA quantification was assayed by a nanodrop spectrophotometer. Multiple chips may be used for one test. For mRNA reverse transcription, 1 μg of RNA was used to synthesize cDNA using RT Primer Mix and Prime Script RT Enzyme Mix I (Takara). The primer sequences including RAC1, forward 5'-GCGTTGCCATTGAACTCACC-3' and reverse 5'-GAGCTGCTACGCTCACTCCATTAC-3'; RhoA, forward: 5'-AGCCTGTGGAAAGACATGCTT-3'; reverse primer: 5'-TCAAACACTGTGGGCACATAC-3'; β-actin forward (5' to 3') : TGCTGTCCCTGTATGCCTCTGG, and β-actin reverse (5' to 3'): ACCGCTCGTTGCCAATAGTGATG were used for the reverse transcriptase of mRNA target. Genes of RhoA and RAC1 were normalized to genes β-actin for mRNA analyses.

### 1.7 PIV analysis and the correlation analysis

The PIVLab toolbox in Matlab is used to run the PIV analysis on the video stack of ICM and the stand-alone (SA) cells. In short, the velocity correlation is calculated by

$$C_{ij} = \left\langle \frac{\overline{V_i(\vec{r})V_j(\vec{r}+\vec{R})} - \overline{V_i(\vec{r})}^2}{\overline{V_i^2(\vec{r})}} \right\rangle$$

as function of the distance $R = |\vec{R}|$, the indices *i* and *j* represent the x- and -y direction. For each image, the correlation function is calculated as a spatial average (over-line) and a second average is taken over time (bracket) sequence of the snapshots.

### 1.8 Reagents and antibodies

For dynamic chemical stimulation, TNF-a input concentration is 1 ng/ml if not otherwise mentioned (Cyagen, US). For the interference of cell-cell connections, the concentrations of used drugs are 1 μM for Jasplakinolide (JASP) (Maokangbio, China); 50 μg/ml E-cadherin antibody (abcam, Shanghai); 50 μM Rac1 inhibitor NSC23766 (MilliporeSigma, US); 10 μM Rho-associated protein kinase (ROCK) inhibitor Y-27632 (abcam, Shanghai); 20 μM cytochalasin D (abcam, Shanghai); 20 μM Blebbistatin (MilliporeSigma, US); 10 μM Cdc42 inhibitor (ML-141) (MilliporeSigma, US); 10 μM Nocodazole (Beyotime, China).

### References


1. M. A. Unger, H. P. Chou, T. Thorsen, A. Scherer, S. R. Quake, Monolithic microfabricated valves and pumps by multilayer soft lithography. Science. 288, 113–116 (2000).
2. Tay, S., Hughey, J.J., Lee, T.K., Lipniacki, T., Quake, S.R., and Covert, M.W. (2010). Single-cell NF-kappaB dynamics reveal digital activation and analogue information processing. Nature 466, 267-271.

# 2. Supplementary information

### 2.1 Cell-cell collision leads to the remodeling of microtubule networks and nuclear deformation

In 2013, Stephen R. Quake, etc. reported that migration of population cells is regulated by cell-cell collision, which results in pseudopod collapse and complex migratory behaviors (*1*). As cell-cell collision causes mechanical cues transduced to the nuclear through cytoskeleton networks (*2*), we expect that the intracellular activities (e.g., the chromatin reorganization) are also affected. To investigate the regulatory effects of cell-cell interactions, different numbers of 3T3 fibroblasts were maintained and monitored in real-time within the shear-free culture chambers of a microfluidic device (Fig. S1 and Fig. S2a). We observed that the migration speed of population cells is substantially lowered at high cell densities (Fig. S2b), where most individual cells are confined by the crowds (Movie S1 and Movie S2). With prolonged incubation at high cell densities >1000/mm$^2$ for 24 h, cell mobility further decreases as compared to the freshly plated cell population (Fig. S2b). Consistently, reconstructed 3D fluorescent images of cytoskeleton networks show that the space in between the neighboring nuclear is mostly occupied by the microtubule networks (Fig. S2h). The lattice network, where fibroblasts are embedded in, is further stabilized by continuous secretion of collagen, which ensures the structural integrity (*3*) and inhibits cell migration (Fig. S2c-e). The fibroblasts eventually self-organize into a monolayer sheet, i.e., the interconnected cell monolayer (ICM), where mechanical cues caused by nuclear migration and shape transition can be effectively transduced the neighbors. Notably, within the crowded cellular environment, changes in the relative position of one cell with respect to another (Fig. S2f), and variations in cell volume (e.g., during cell division) (Fig. S2g) lead to nuclear deformation of neighboring cells. While, in the less crowded cellular environment, cell-cell collision mostly results in cell and nuclear translocation (Fig. S2k and S2l). Estimated by overlapping nuclear outlines at different time points, we demonstrated that the occurrence of nuclear shape transitions, whose amplitude is greater than 10% of the total area, is considerably higher in ICM than the stand-alone (SA) population cells (Fig. S2i and S2j). These results demonstrate that cell-cell collision in the crowded cellular environment leads to nuclear deformation, and the transduction of mechanical forces from one nuclear to another indicates that the space in between is fully occupied. Intriguingly, the occurrence of cell-cell collision and the nuclear deformation in ICM further decreases with prolonged incubation (Fig. S2b and S2i), suggesting stronger confinement and intercellular connectivity (Fig. S2m).

### 2.2 Collective activities in ICM is mediated by the interconnective actin filaments

We then analyzed the velocity field in ICM using OpenPIV, an open source particle image velocimetry (PIV) software (Fig. S2n) (*4*). With the window size of ~ 60 μm by 60 μm, we observed that collective activities emerge in the displacement of nuclear at cell densities higher than 400 cells/mm$^2$ (Fig. S2o-p), showing correlation distance $R$ up to nearly 70 μm. As cell-cell connection, which is mediated by cadherins and actin filaments (*5*), plays central roles in regulating collective migration of population cells (*6*), we then looked at the collective behavior of actin networks in the ICM. It was observed that at a cell density of ~ 500 cells/mm$^2$, actin filaments are highly interconnective and mobile at the initial stage of culture on chip (Fig. S2q-s and Movie S3). Collective behavior emerges instantaneously at 0 h, showing correlation length of ~ 60 μm (Fig. S2r). After 24-hour incubation, the mobility of actin filaments decreases dramatically (Fig. S2q and Movie S3), which is consistent with the declined cell mobility observed in the ICM shown in Fig. S2b. In the meantime, the collective behavior remains, showing correlation length of ~ 70 μm (Fig. S2s). These results suggest that the collective activities and the propagation of mechanical cues within the ICM is mediated by the collective movement and deformation of actin filaments, which changes the intra-cellular mechanical loads.

### 2.3 Dynamic mechanical cues reflected by morphological features of individual cells

The dynamic mechanical cues can be reflected by changes in the morphological features of individual cells (Fig. S2t-v). For example, the shape changes of the whole cell reflect changes in the extension of actin filaments ($\Delta l$), which lead to diminished stress on the nuclear (Fig. S2t), and reorganization of microtubule networks (Fig. S2u), resulting in either nuclear deformation or displacement depending on the cellular environment. The mechanical

forces from actin filaments can be simplified using $f_{actin} = \sum_{n=1}^{N_{actin}} k_{actin} \cdot \Delta l_n$, where $N_{actin}$ is the number and $k_{actin}$ is the linear elastic coefficient of the deformed actin filaments. As microtubules are ~300 times stiffer than actin filaments (*7*), the microtubule networks transduce mechanical cues from ECM and neighboring cells without buckling. Since the microtubule fills in volume of individual cells (Fig. S1f-h) and shows no sign of interconnection between neighboring cells, the remodeling of microtubule networks can be directly reflected by cell shape changes (Fig. S2h). In the meantime, the space in between cells is filled by collagen in ICM (Fig. S2e), and the volume between individual nucleus is mostly filled by microtubule (Fig. S2f-h). The movement and deformation of individual cell can directly affect its neighbors (Fig. S2f-g). Changes in the relative position of one cell with respect to another (Fig. S2f), and variations in cell volume (e.g., during cell division) (Fig. S2g) can therefore cause cytoskeleton remodeling and nuclear deformation of neighboring cells. We estimated the mechanical forces by measuring the total area changes between cells (Fig. S2u). For example, with unchanged $d_1$ and $d_2$, the variation in the distance between Cell 1 and Cell 3 brings changes in the area in between three cells $\Delta S_{microtubule} + \Delta S_{collagen}$ and elastic force $F_{triangle} = k_m \cdot \Delta S_{microtubule} + k_c \cdot \Delta S_{collagen}$, where $k_m$ and $k_c$ are the surface elastic coefficients. Notably, the mechanical forces are delivered to all cells in direct contact of the triangular area. Considering the fact that cell membrane is considerably softer than the cytoskeleton elements, the effect of dynamic variations in membrane surface tension caused by the changing cell area is neglectable.

Besides cytoskeleton remodeling, the depolymerization of actin filaments can also generate intra-cellular mechanical cue and cause nuclear deformation (Fig. S2v). Shivashankar, et al. reported that simultaneously with the biochemical signaling events (e.g., NF-κB nuclear localization), TNF-α stimulation activates mechano-signaling and causes actin depolymeri-zation (*8*), which changes the mechanical loads on the nuclear.

**2.4 Propagating mechanical cues estimated by cell movement trajectories**

To evaluate the TNF-α-stimulated contractile actions of ICM, the trajectory of individual cell ($x_1$, $x_2$, … $x_n$) and ($y_1$, $y_2$, … $y_n$), where n is the total frame number, is averaged every 5 to 10 steps depending on the frame rate, e.g., $x_i^{'} = (x_{i+1} + x_{i+1} + \cdots x_{i+5})/5$ and $y_i^{'} = (y_{i+1} + y_{i+1} + \cdots y_{i+5})/5$. The deviation of cell migration coordinates from the averaged trajectory Δl can then be calculated from its minimum distance to the piecewise cubic interpolation curve of $(x_1^{'}, x_2^{'}, \cdots x_{n/5}^{'})$ and $(y_1^{'}, y_2^{'}, \cdots y_{n/5}^{'})$ (Fig. S3l).

**2.5 Calculation of correlation between the responses of neighboring cells**

In this study, the correlation of signaling and morphological responses has been calculated, e.g., between the morphological responses of neighboring cells (Fig. 1p), between the periodic TNF-α and morphological response (Fig. 1q), between cytoskeleton remodeling and NSF (Fig. 2c-d), between NSF of neighboring cells (Fig. 2j). For instance, when we calculated the correlation of NF-κB nuclear localization dynamics between two neighboring cells, the cross-correlation function can be defined as:

$$correlation(\Delta t) = \overline{NF_1^{'}(t) NF_2^{'}(t+\Delta t)} \Big/ \sqrt{\overline{\left[NF_1^{'}(t)\right]^2} * \overline{\left[NF_2^{'}(t+\Delta t)\right]^2}}$$

where $NF_1(t)$ and $NF_2(t+\Delta t)$ are the nuclear NF-kB fluorescence intensity in cell 1 and 2, respectively. $NF_1^{'}(t) = NF_1(t) - \overline{NF_1(t)}$ and $NF_2^{'}(t+\Delta t) = NF_2(t+\Delta t) - \overline{NF_2(t+\Delta t)}$ are the fluctuations of NF-kB signals in cell 1 and 2, where $\bar{\cdot}$ indicates temporal averaging accordingly.

## References


1. S. Vedel, S. Tay, D. M. Johnston, H. Bruus, S. R. Quake, Migration of cells in a social context. *Proceedings of the National Academy of Sciences* **110**, 129 (2013).

2. F. Alisafaei, D. S. Jokhun, G. V. Shivashankar, V. B. Shenoy, Regulation of nuclear architecture, mechanics, and nucleocytoplasmic shuttling of epigenetic factors by cell geometric constraints. *Proceedings of the National Academy of Sciences of the United States of America* **116**, 13200-13209 (2019).

3. K. Gelse, E. Pöschl, T. Aigner, Collagens--structure, function, and biosynthesis. *Advanced drug delivery reviews* **55**, 1531-1546 (2003).

4. Z. J. Taylor, R. Gurka, G. A. Kopp, A. J. I. T. o. I. Liberzon, Measurement, Long-duration time-resolved PIV to study unsteady aerodynamics. *IEEE Transactions on Instrumentation Measurement* **59**, 3262-3269 (2010).

5. M. Cavey, T. Lecuit, Molecular bases of cell-cell junctions stability and dynamics. *Cold Spring Harbor perspectives in biology* **1**, a002998 (2009).

6. J. M. Wood, M. F. Olson, Collective migration: spatial tension relief. *Current biology: CB* **22**, R125-127 (2012).

7. T. J. Mitchison, Compare and contrast actin filaments and microtubules. *Molecular biology of the cell* **3**, 1309-1315 (1992).

8. A. Mitra *et al.*, Cell geometry dictates TNFα-induced genome response. *Proceedings of the National Academy of Sciences of the United States of America* **114**, E3882-e3891 (2017).

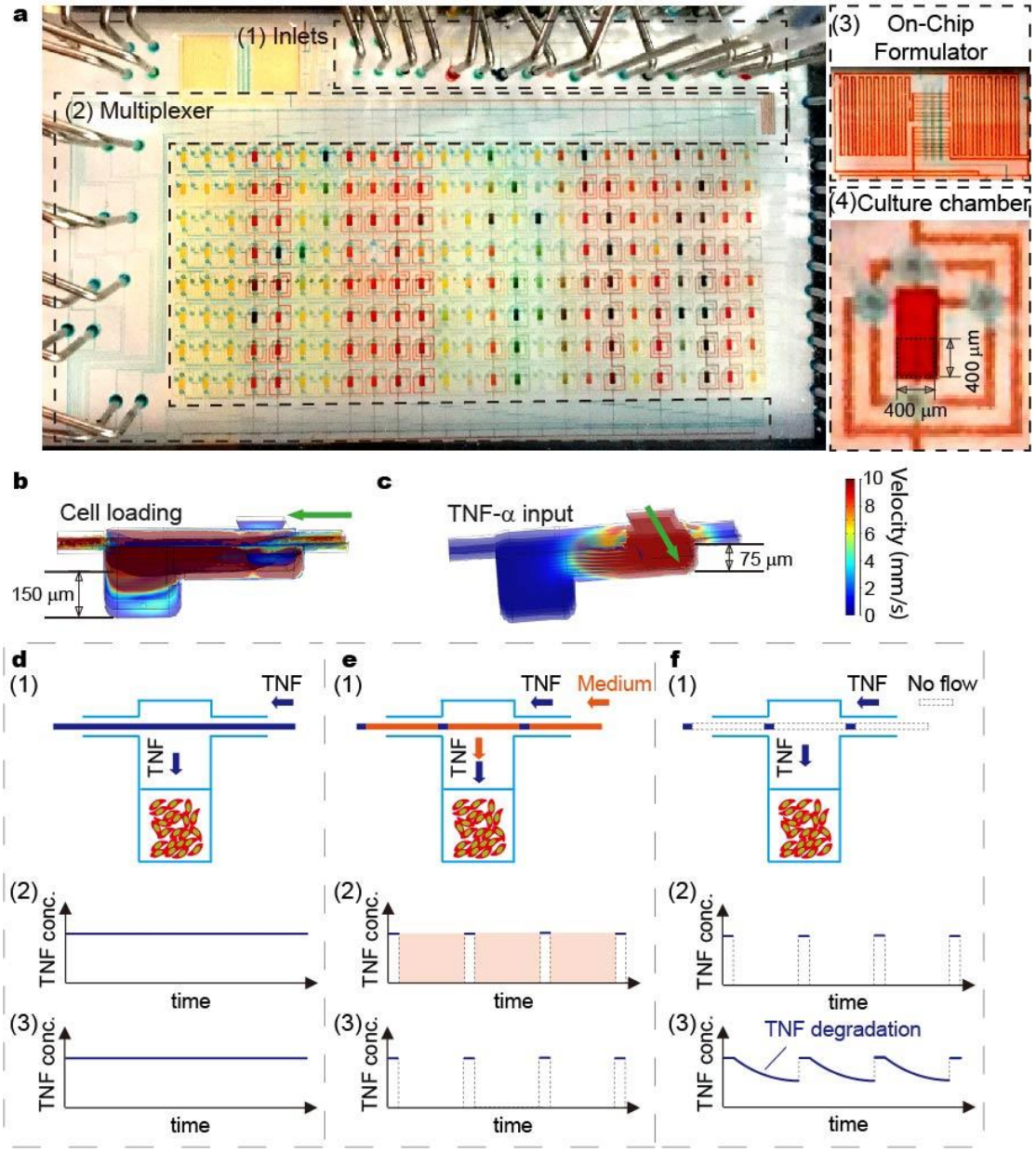


Figure S1 Fibroblasts in ICM and stand-alone (SA) cells are maintained in a shear-free microfluidic device, Related to Figure 1a. a, Automated cell culture system for dynamical live-cell analysis. (1) The microfluidic device contains 15 inlets; (2) a multiplexer, which allows control of 200 culture units; (3) an on-chip formulator with nanoliter accuracy; (4) and shear-free culture units controlled by 4 active valves (blue). The culture units are composed by 2 parts, a culture chamber of 400μm×400μm×150μm in dimension and a buffering level of 400 μm×400μm×75μm. b, Two-layer cell culture chamber allows firstly quick cell loading. c, Nutrients and TNF-α are delivered to cells in a shear-free manner. d-f: Dynamic inflammatory signals generated using microfluidic module: d, Continuous delivery of fresh TNF-α solution to cultured cells in diffusion-based mode maintain TNF-α concentration in cellular microenvironment. e, Timely replacement of TNF-α solution by culture medium allows generation of pulsatile TNF-α input. f, Programed delivery of TNF-α solution generated damped oscillatory TNF-α signal due to TNF-α degradation.

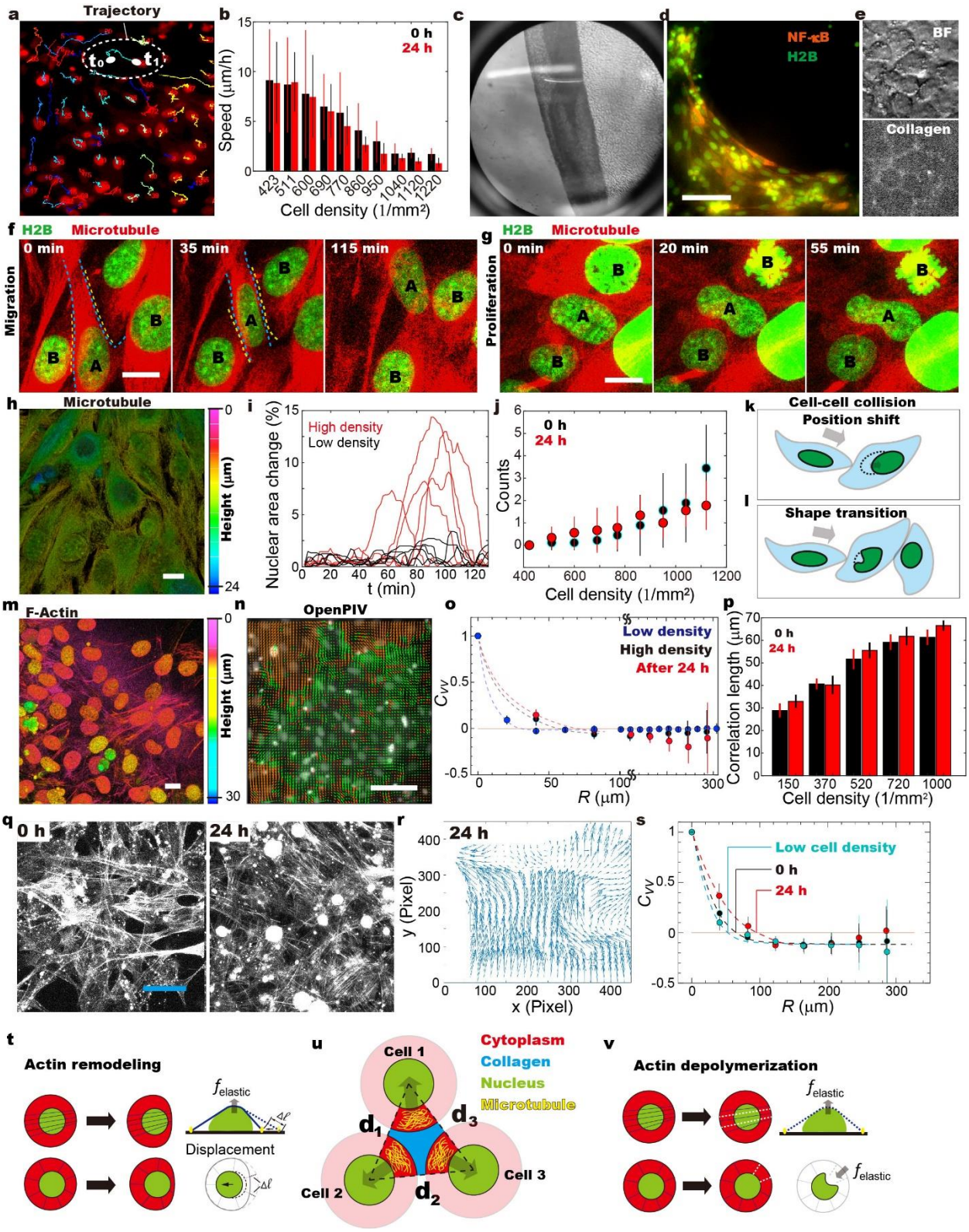
a
Trajectory
b
Speed (μm/h)
0 h
24 h
Cell density (1/mm²)
c
d
NF-κB
H2B
e
BF
Collagen
f
H2B
Microtubule
Migration
0 min
35 min
115 min
g
H2B
Microtubule
Proliferation
0 min
20 min
55 min
h
Microtubule
Height (μm)
i
Nuclear area change (%)
High density
Low density
t (min)
j
Counts
0 h
24 h
Cell density (1/mm²)
k
Cell-cell collision
Position shift
l
Shape transition
m
F-Actin
Height (μm)
n
OpenPIV
o
Cvv
Low density
High density
After 24 h
R (μm)
p
Correlation length (μm)
0 h
24 h
Cell density (1/mm²)
q
0 h
24 h
r
24 h
y (Pixel)
x (Pixel)
s
Cvv
Low cell density
0 h
24 h
R (μm)
t
Actin remodeling
f elastic
Displacement
u
Cell 1
Cell 2
Cell 3
Cytoplasm
Collagen
Nucleus
Microtubule
d1
d2
d3
v
Actin depolymerization
f elastic
f elastic

Figure S2. Dynamic mechanical cues caused by cytoskeleton reorganization in the ICM, Related to Figure 1a-b. a. Trajectories of 3T3 fibroblast nuclear centroids show distinctive mobilities of single cells in the interconnected cell monolayer (ICM). b. Mobility of individual cells were evaluated by measuring the displacement of nuclear in 1 hour. It is demonstrated that cell mobility drops substantially at high cell density, i.e., higher than 1000 cells/mm$^2$. There are at least 5 repeats for each cell density. c. Folded ICM layer in 96-well plate shows that fibroblasts form a connective sheet. d. ICM layer maintained in the shear-free microfluidic chip (see also Supplementary Video 1). e. Bright field (BF) and fluorescent images showing that the gaps between neighboring cells are filled by collagen fibers. f,g Representative confocal fluorescence images of nuclear deformation, (c) when cell-A passed the gate of 2 cell-B, and (d) when there is considerable volume increase in the neighboring cell-B due to division. h. Reconstructed 3D image of the nucleus and microtubule networks, where color represents height of the structure, demonstrate that the microtubule networks fill in the volume surrounding the nucleus. i. Comparison of nuclear shape transition (i.e., the absolute value of nuclear area changes) at low (dark lines) and high cell densities suggests that nuclear deformation is considerably amplified in the crowded cellular environment. j. The number of cells, which go through nuclear shape change over 10% in amplitude, shows close correlation with the cell density. k,l. Schematic shows that cell-cell collision leads to nuclear translocation of neighboring cells at low cell density (k), and nuclear shape transition at high cell density (l). m. Reconstructed 3D image of the nucleus and actin filaments demonstrate that actin locates mostly at the bottom of the ICM. n. Velocity field of nuclear movement in ICM, which was analyzed using OpenPIV software. o. Correlation between velocity vectors of nuclear indicates that mechanical cues from one cell can be transduced to other cells, which are ~ 60 μm away. p. The correlation length of nuclear velocity field linearly correlates with the cell density, which can be up to 70 μm in ICM. q. Fluorescent images of the actin filaments in ICM at different timepoints after being plated in the 96-well plate. r. Velocity field of actin filaments in ICM after 24 h. s. Correlation between velocity vectors of actin networks indicates that the collective movement in ICM is mediated by the interconnective actin filaments, which reaches ~ 60 μm at the initial stage of culture on chip. t. Schematic shows that cell shape changes lead to remodeling of actin filaments, resulting elastic forces on the nuclear. u. Cell-cell collision in the crowded environment leads to deformation in microtubule and collagen networks, which transduces mechanical forces to the nuclear. The dynamic mechanical cues can be estimated by measuring the cell-cell distance, and the triangular area in between three nuclear. v. Actin depolymerization leads to changed mechanical loads on the nuclear, and consequently causes nuclear deformation. Scale bars denote 50 μm in Fig. d; 10 μm in Fig. f, Fig. g, Fig. h and Fig. m; 100 μm in Fig. n; 40 μm in Fig. q.

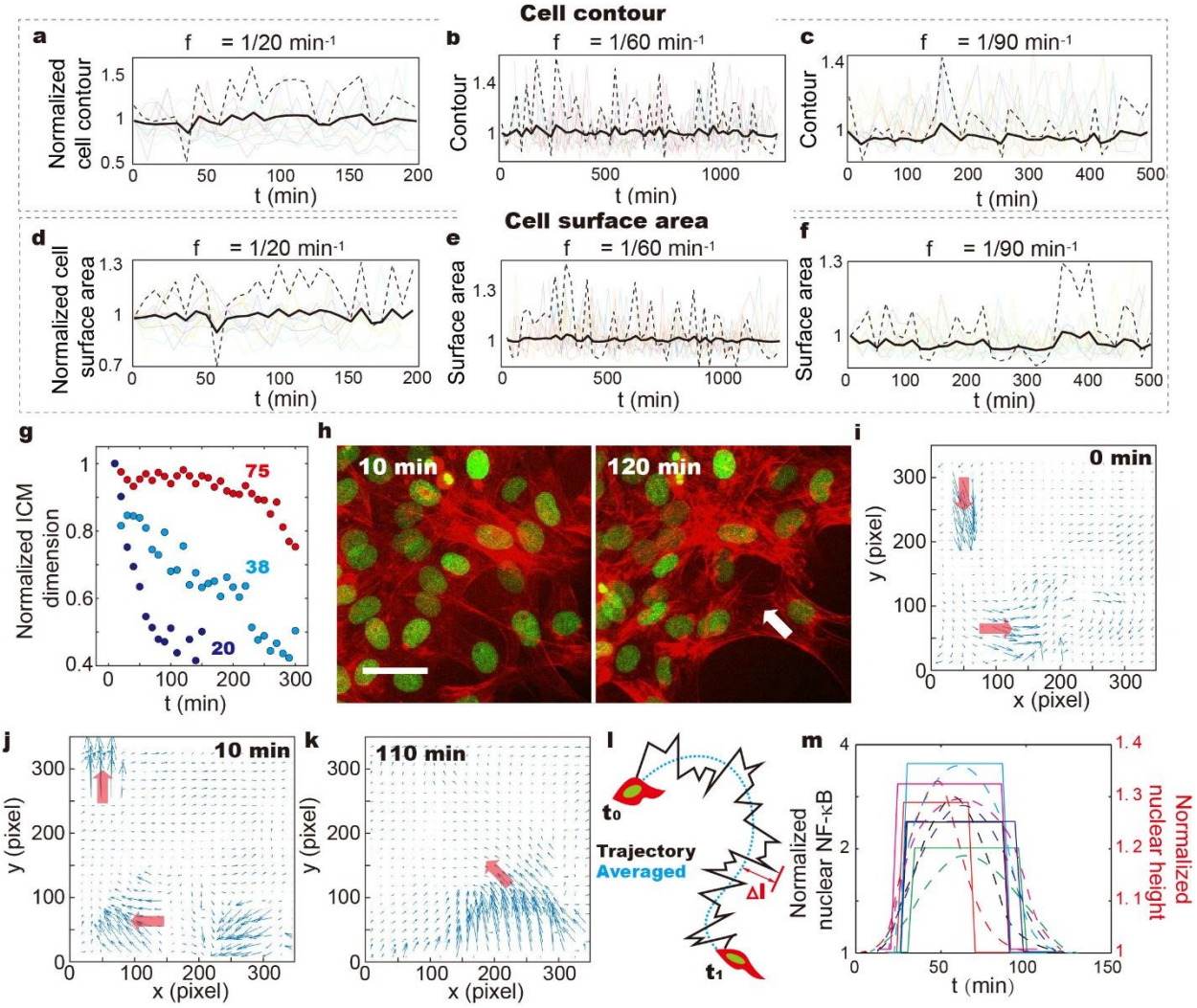


Figure S3. Morphological responses of fibroblasts in the interconnective cell monolayer (ICM), Related to Figure 1p-q. a-c. Measuring the perimeter of individual cells in ICM reveal the line strain, which shows no collective behavior. d-f. The variations in 2D area of single cell surface reflect the fluctuating surface tension. In Fig. a-f, The translucent lines are traces of individual cells. The solid lines are the average of all single cell traces, and the dashed line is the enlarged view of the solid line for better visualization of the fluctuation. g. The contractile behavior depends on the size of ICM. All values in the traces were normalized by the initial ICM dimension before TNF-α stimulation. For example, the ICM containing ~20 cells shrink down to ~40% of its original size. h. Representative confocal fluorescence images at the edge of ICM. As is indicated in Movie S5, the contractile activities are initiated by the detachment of actin filaments from cell-cell and cell-ECM connections (indicated by the arrow). i-k. Velocity field of actin filaments in ICM at the marginal area of ICM. l. ICM deformation is evaluated by measuring the distance of cell migration trajectory to the averaged curve, fluctuation of which reflect vibration of nuclear centroids. m. Variations in the nuclear height (solid lines) coordinate with the NF-κB dynamics (dashed lines). Scale bar denotes 20 μm.

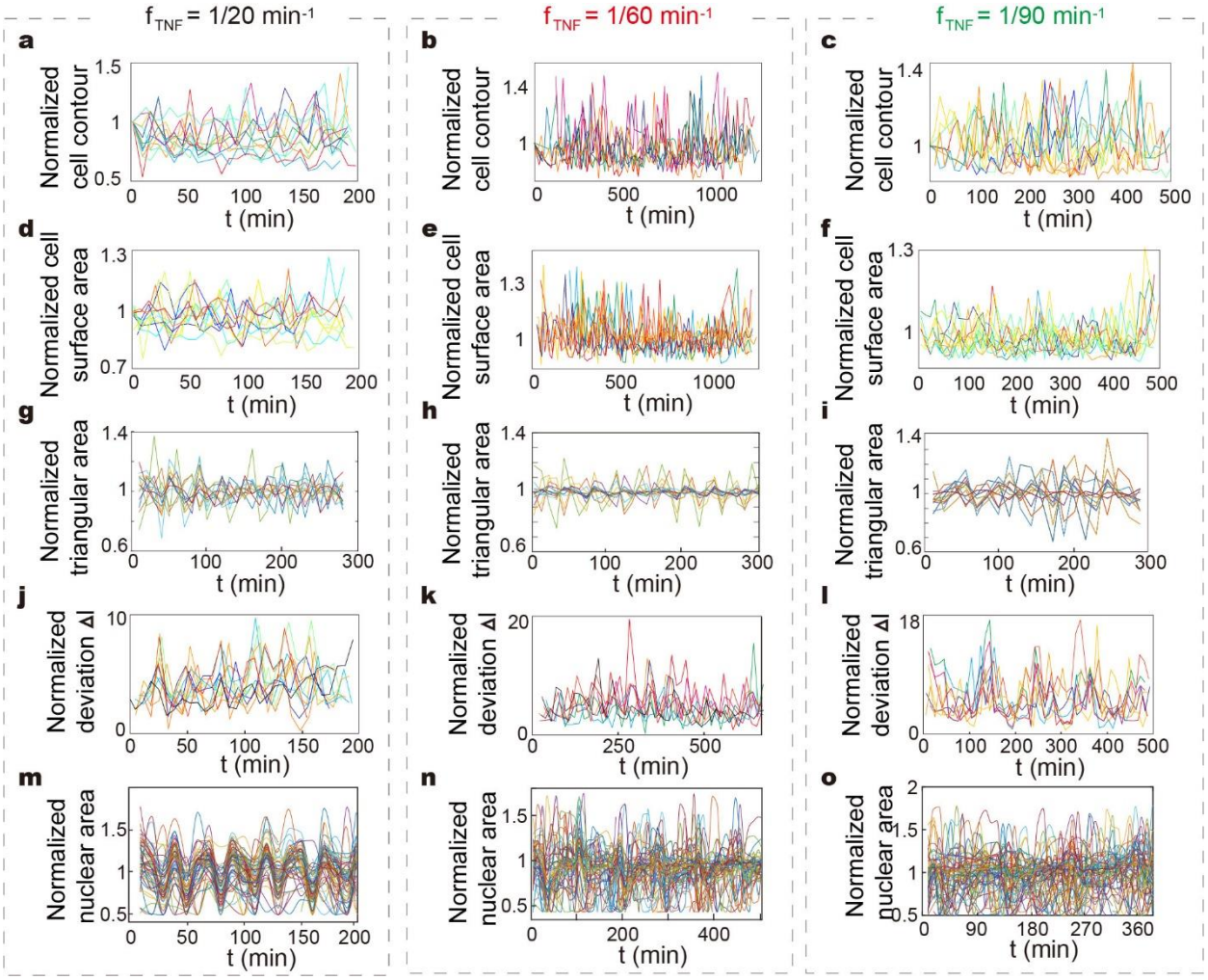


Figure S4: Morphological response of population cells in ICM upon periodic TNF-α stimulation, Related to Figure 1c-e, g-i, k-m and o-q. (a-c) Contour, (d-f) 2D surface area of individual cells in ICM changes during 1/20 $min^{-1}$, 1/60 $min^{-1}$ and 1/90 $min^{-1}$ TNF-α stimulation. (g-i) Relative displacement of nuclear with respect to the neighbors causes changes in the triangles area shown in Fig. 1a, which reflect the cell-cell and cell-ECM interactions. (j-l) Collective vibration of nuclear centroids in ICM reflects deformation of cell monolayer, which coordinates with periodic TNF-α stimulation. (m-o) Nuclear shape fluctuation (NSF) traces of single fibroblasts in ICM upon periodic TNF-a stimulation. For better visualization, all contours were normalized to initial value of individual cells, and other morphological features normalized by the average value of individual traces. Traces from individual cells are color coded.

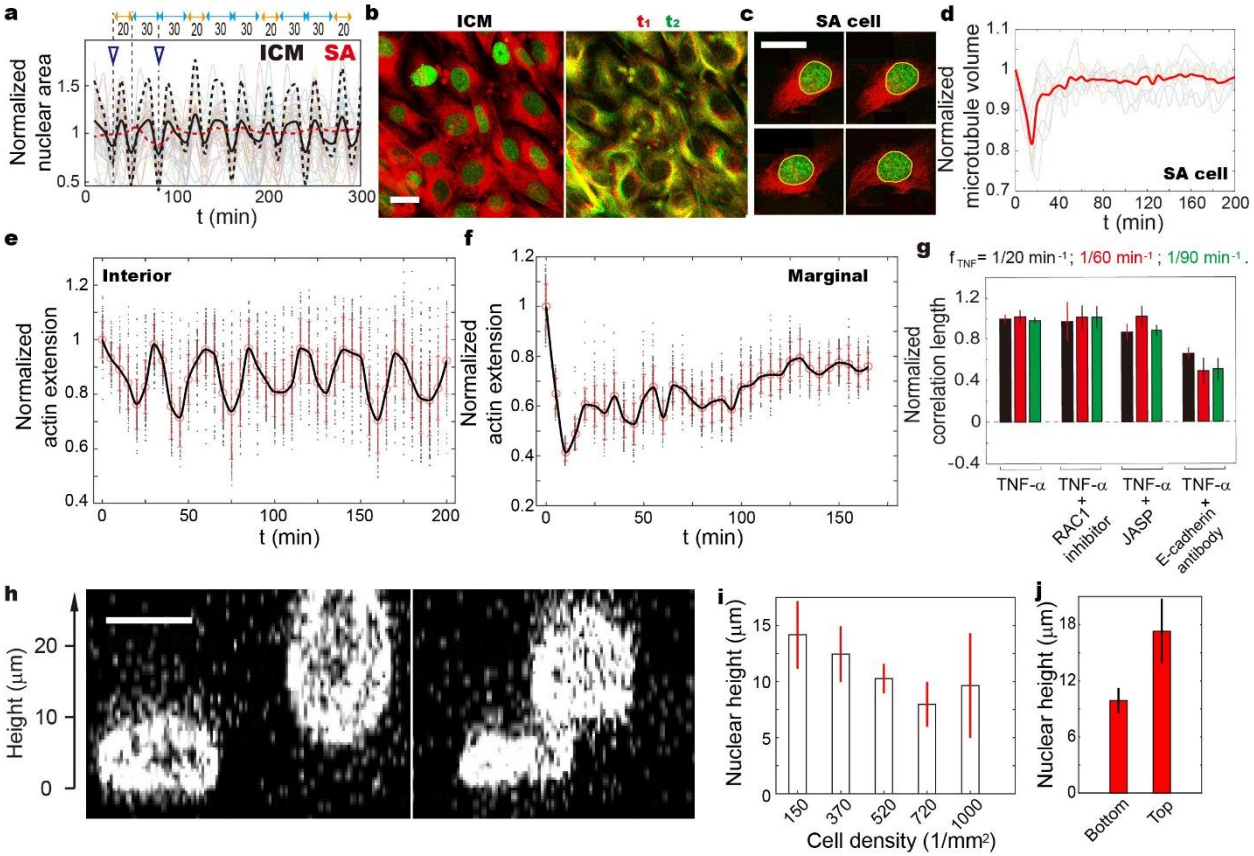


Figure S5. Cytoskeleton reorganization of fibroblasts in ICM and the SA cells upon TNF-α stimulation, Related to Figure 1o and Figure 2j. a. NSF traces of single fibroblasts in ICM upon stimulation by 1/20 $min^{-1}$ TNF-α input. The individual NSF were normalized by the average value of each trace. The translucent lines are the traces of all participating cells, and the solid line is the averaged value of all traces. The red dashed lines represent averaged trace of stand-alone (SA) fibroblasts. b. Representative fluorescent images of the ICM, where nuclear (green) and microtubule (red) are immune-stained, demonstrate that there are no obvious volume changes in the microtubule of individual cells. c. Stand-alone (SA) cell show decrease in size when being firstly in contact with TNF-α. Elevated level of the microtubule fluorescence intensity suggest increases in the local density. d. Traces of the microtubule volume of individual cells reveal that the microtubule network remodeling of population cells in ICM are not coordinated. The traces were normalized by the initial value for better visualization. e,f. By measuring the extension of actin filaments (black dots) of individual cells in ICM and stand-alone (SA) cells, our studies reveal that deformation of actin filament leads to variations in the mechanical loads on the nuclear. In contrast to the ~20% value of the averaged actin extension, the fluctuation amplitude of SA cells is less than 10% upon periodic TNF-α stimulation, and thus considerably smaller mechanical forces on the nuclear. The traces were normalized by the initial value for better visualization. The black dots are the extension of individual actin filaments. The red circles and bars are the average value of individual cell's actin filaments and the standard deviation, respectively. The black lines are the smoothed traces of variations in actin extension. g. Correlation length of ICM shows that the collective movement of actin filaments is disrupted by E-cadherin antibody, which disrupts cell-cell connections. All values were normalized to the control value, which was obtained by treating ICM with only 1/20 $min^{-1}$ TNF-α. h. Cross-sectional images demonstrate that cells sitting on the PDMS substrate show considerably lower height than the ones at the top of ICM. i. The height of the nuclear is inversely correlate with the cell density, suggesting the formation cell-cell connection causes compressive forces on the nuclear. j. Cells embedded in the interconnective actin networks (Bottom) show an average height of ~ 7 μm, which is considerably lower than the ones sitting on top of ICM, i.e., ~ 15 μm. Scale bars represent 20 μm.

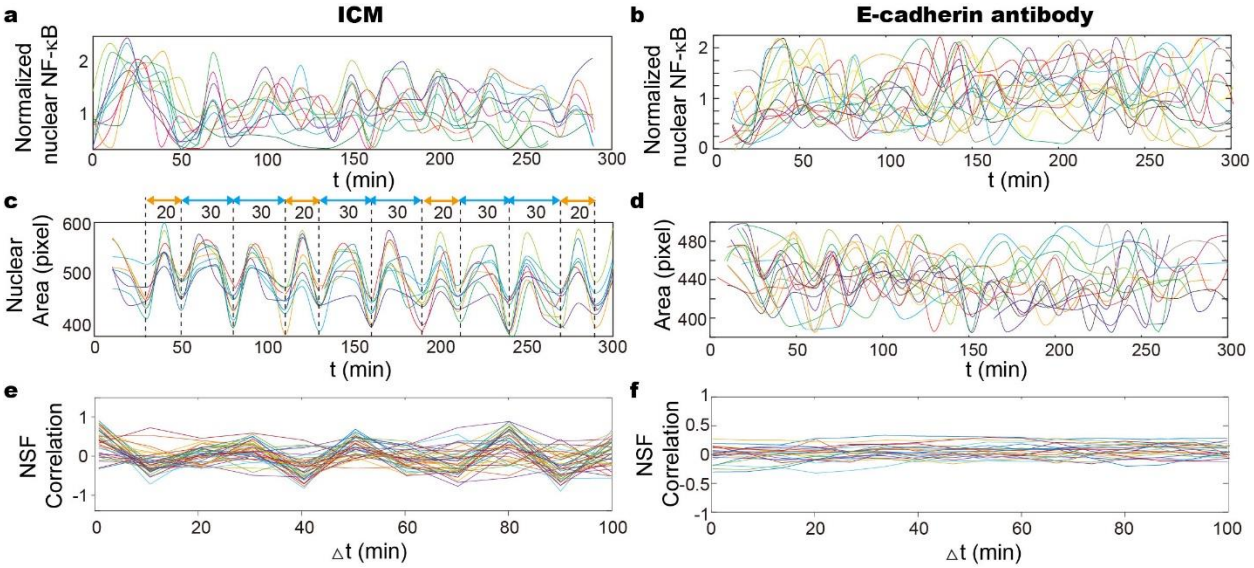


Figure S6: The collective activities in response to TNF-α stimulations were disrupted with the addition of E-cadherin antibody, Related to Figure 2j. a-d. Traces of variations in nuclear NF-κB and nuclear area show that the nuclear localization of NF-κB transcription factor is synchronized in ICM with 1/20 $min^{-1}$ TNF-α stimulation (a,c). The synchronization as well as the formation of ICM is disrupted with the addition of E-cadherin antibody (b,d). Nuclear NF-κB traces were normalized by the average value. e,f. Cross-correlation analysis between NSF time traces of neighboring cells shows that when lag Δt=0, the NSF of individual cells positively correlate with their neighbors with 1/20 $min^{-1}$ TNF-α stimulation (e). While, the distribution seems to center at zero with the addition of E-cadherin antibody (f), suggesting collective NSF is disrupted when cell-cell interconnections are blocked. Traces from individual cells are color coded.

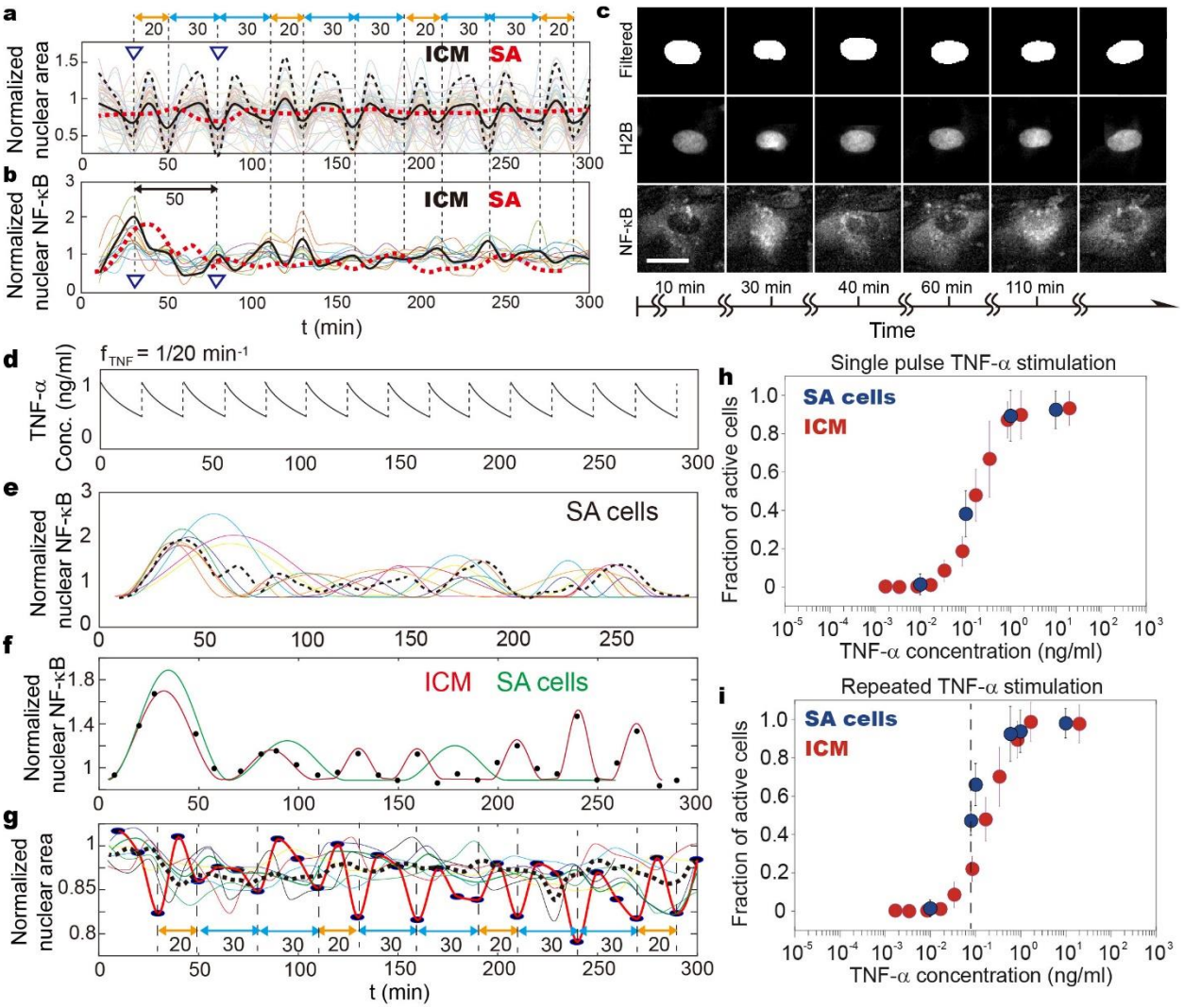


Figure S7. Responsiveness of fibroblasts in ICM and the SA cells, Related to Figure 4a-d. a,b. NF-κB and NSF traces of single fibroblasts in ICM upon stimulation by 1/20 $min^{-1}$ TNF-α input. Solid lines reflect NF-κB dynamics and nuclear area variances averaged among all participating cells. The black dashed lines are the enlarged view of those solid lines, showing subtle variations in NSF, and the red dashed lines represent averaged NF-kB trace of stand-alone (SA) fibroblasts. c. NF-κB dynamics and NSF of single cells in ICM are monitored in real-time using fluorescence microscopy. Images show NF-κB (p65-dsRed) nuclear localization and nuclear shape changes upon periodic TNF-α stimulation. The images of H2B-GFP are processed using real-space bandpass filters to extract morphological features including perimeter and area, etc. d-g. NF-κB dynamics and NSF traces of ICM and SA cells when being exposed to 1/20 $min^{-1}$ TNF-α stimulation. It is demonstrated collective activities only emerge in ICM, where amplitude of NSF and NF-κB oscillation is greatly elevated. In Fig. e, the traces of individual cells are presented as the color-coded solid lines, and the dashed line is the average of all traces. In Fig. f, the averaged traces of NF-kB dynamics of ICM (red) and SA cells (green) are compared. In Fig. g, the color-coded solid lines are the nuclear area traces of SA cells. The dashed line is the average of all SA cell traces. The black dots and red solid line are the averaged trace of population cells in ICM. h-i. Fraction of cells responding to single pulse, and repeated TNF-α stimulation (1/20 $min^{-1}$ frequency). It is demonstrated that similar number of fibroblasts in ICM (blue) respond to single pulse TNF-α stimulation as the SA cells (red). While, higher number of responsive cells was observed in ICM as compared to SA cells upon stimulation by repeated TNF-α stimulation. The dashed line shows the position of 0.08 ng/mL TNF-α concentration. The NSF and NF-κB traces were normalized by their average value. Scale bar in Fig. c denotes 20 μm.

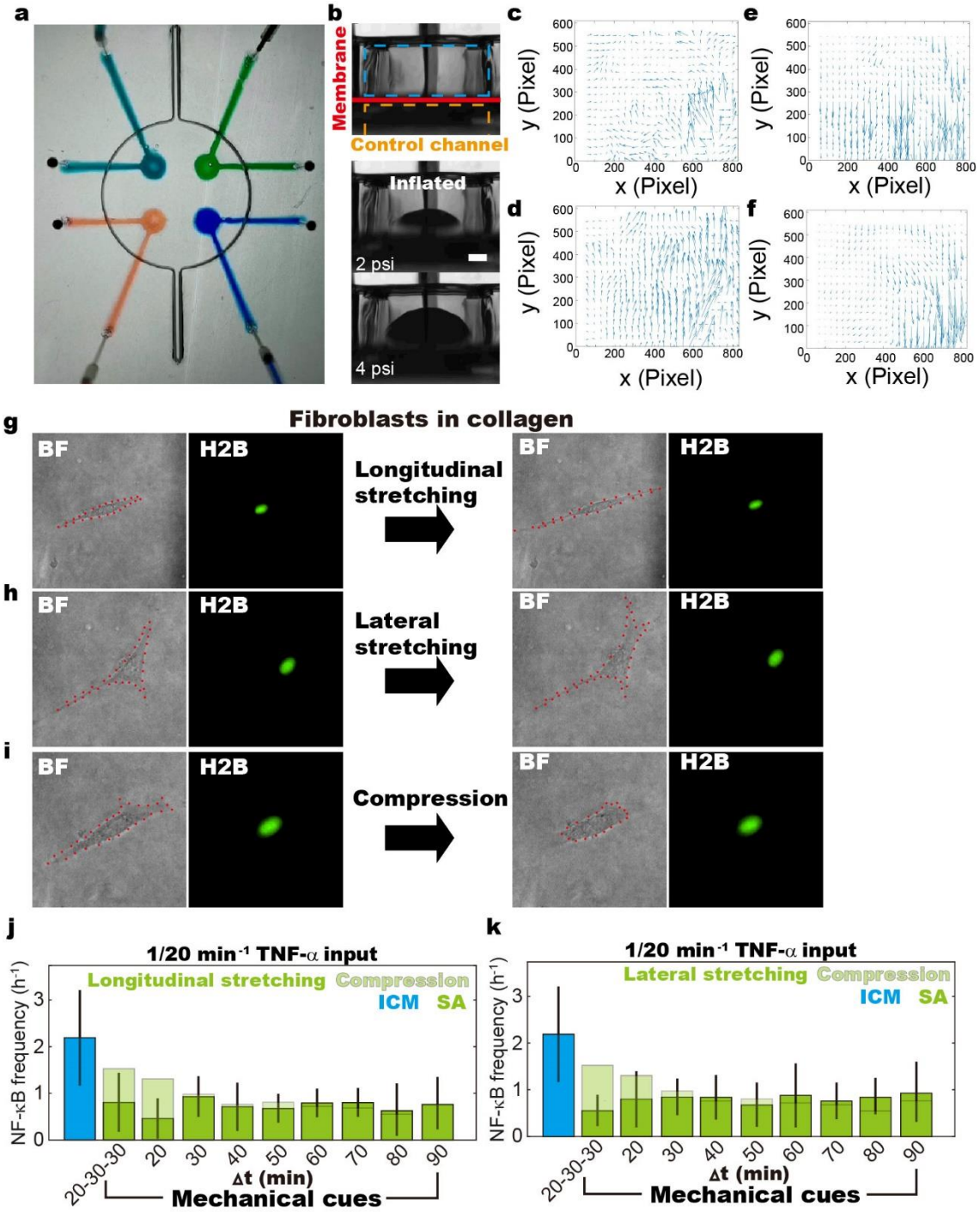


Figure S8. Morphological transitions of stand-alone (AS) cells induced by pressurizing the PDMS membrane, and consequently the remodeling of collagen fibers, Related to Figure 5a-b and d. a. The microfluidic chip is composed by a 4 stretchable PDMS membrane at the bottom of the culture chamber. b. Cross-sectional view of the fluidic chip with stretchable PDMS membrane. Fibroblasts are loaded, and maintained in the culture chamber (blue). PDMS membrane (red) is stretched by pressurizing the control channel (orange). Stretched PDMS membrane at pressure of 2 psi (left) and 4 psi (right). Scale bar denotes 200 μm. c-f. Distribution of the velocity field in the collagen matrix, which is generated by pressurizing different PDMS membranes, suggests various mechanical cues. g-i. Mechanical cues including pulling, stretching and compression are delivered to SA cells by inducing remodeling of collagen fibers.

j-k. By simultaneously introducing 1/20 $min^{-1}$ TNF-α and different frequencies of collagen remodeling ranging from 1/20 to 1/90 $min^{-1}$, the effect of ICM contraction on NF-κB dynamics is systematically studied. It is revealed that when cells are either pulled or stretched, the induced mechanical cues bring no obvious changes as compared to the SA cells with no induced morphological transitions. Scale bar in Fig. b denotes 200 μm.

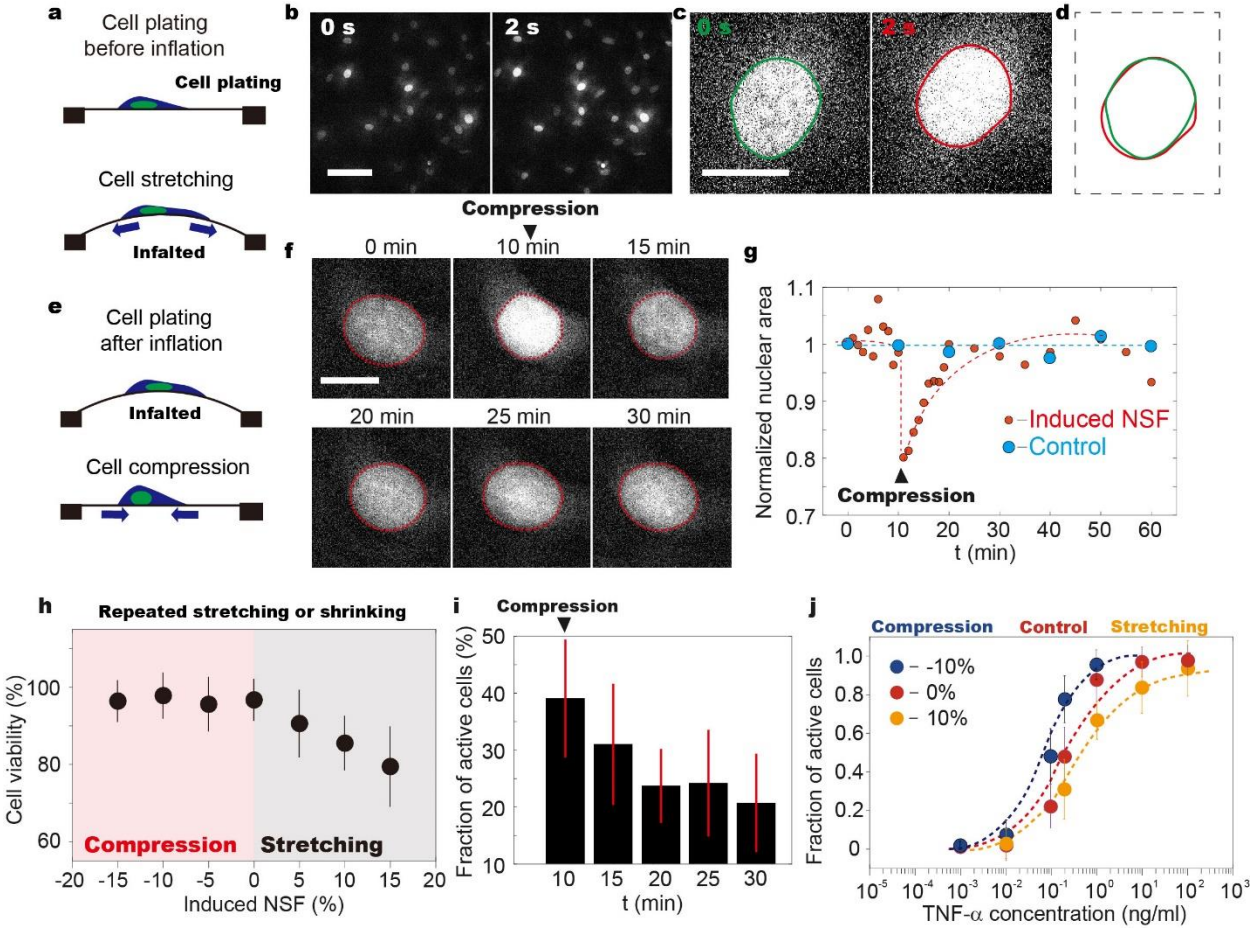


Figure S9. Responsiveness of SA cells with induced NSF, Related to Figure 6a. a. Schematic view showing that cell adhesion surface can be stretched when being plated on relaxed PDMS membrane, which is later inflated. b,c. Fluorescent images cells plating on a relaxed PDMS membrane, which is later inflated. d. Comparison between the outlines of individual cell at different timepoints shows distinctions in nuclear shape and area. e. To reach a relaxed state for the actin networks, cells were plated on an inflated PDMS membrane surface, which were then relaxed. f. Representative fluorescence images of nuclear shrinkage with decreased adhesion area. Cell gradually restore its original conformation within 20 min. g. Single cell traces showing nuclear shape variances with decreased (red) and unchanged (blue) adhesion area. All values were normalized by the initial nuclear area. The dashed lines were drawn for better visualization. h. Cell viability when being placed on repeatedly stretched or shrunk (at frequency of 1/20 $min^{-1}$) PDMS membrane for 2 hours. It is demonstrated that fibroblasts viability remains similar to control (~100%) when cell adhesion area repeatedly decreases. Cell viability decreases when being stretched, suggesting DNA damage induced by increased osmotic pressure at the top of chromatin. i. Responsiveness of fibroblasts to 0.1 ng/mL TNF-α stimulation at different stages of induced nuclear shape change. It is demonstrated that the increased responsiveness upon nuclear shape changes is only temporal. Fibroblasts restore the characteristics of isolated cells after 5 to 10 min. j. Fibroblasts are less responsive to TNF-α stimulation (single pulse) when nuclear area laterally expands by ~10%, and more when nuclear area decreases (~-10%). Scale bars denote 50 μm in Fig. b and 10 μm in Fig. c and Fig. f.